

# VOID STATISTICS IN LARGE GALAXY REDSHIFT SURVEYS: DOES HALO OCCUPATION OF FIELD GALAXIES DEPEND ON ENVIRONMENT?

JEREMY L. TINKER<sup>1,2</sup>, CHARLIE CONROY<sup>1,3</sup>, PEDER NORBERG<sup>4</sup>,  
SANTIAGO G. PATIRI<sup>5</sup>, DAVID H. WEINBERG<sup>6</sup>, & MICHAEL S. WARREN<sup>7</sup>

*Draft version October 30, 2018*

## ABSTRACT

We use measurements of the projected galaxy correlation function  $w_p(r_p)$  and galaxy void statistics to test whether the galaxy content of halos of fixed mass is systematically different in low density environments. We present new measurements of the void probability function (VPF) and underdensity probability function (UPF) from Data Release Four of the Sloan Digital Sky Survey (SDSS), as well as new measurements of the VPF from the full data release of the Two-Degree Field Galaxy Redshift Survey. We compare these measurements to predictions calculated from models of the Halo Occupation Distribution (HOD) that are constrained to match both the projected correlation function  $w_p(r_p)$  and the space density of galaxies  $\bar{n}_g$ . The standard implementation of the HOD assumes that galaxy occupation depends on halo mass only, and is independent of local environment. For luminosity-defined samples, we find that the standard HOD prediction is a good match to the observations, and the data exclude models in which galaxy formation efficiency is reduced in low-density environments. For  $L_*$  samples we cannot rule out a slight increase in galaxy formation efficiency at low densities. More remarkably, we find that the void statistics of red and blue galaxies (at  $L \sim 0.4L_*$ ) are perfectly predicted by standard HOD models matched to the correlation function of these samples, ruling out “assembly bias” models in which galaxy color is correlated with large-scale environment at fixed halo mass. We conclude that the luminosity and color of field galaxies are determined predominantly by the mass of the halo in which they reside and have little direct dependence on the environment in which the host halo formed. In broader terms, our results show that the sizes and emptiness of voids found in the distribution of  $L \gtrsim 0.2L_*$  galaxies are in excellent agreement with the predictions of a standard cosmological model with a simple connection between galaxies and dark matter halos.

*Subject headings:* cosmology:theory — galaxies:halos — large scale structure of the universe

## 1. INTRODUCTION

The Halo Occupation Distribution (HOD) has become one of the primary methods for analyzing and interpreting galaxy clustering measurements (e.g., Kauffmann et al. 1997; Jing et al. 1998; Benson et al. 2000; Seljak 2000; Peacock & Smith 2000; Ma & Fry 2000; Scoccimarro et al. 2001; Berlind & Weinberg 2002). The unique and powerful aspect of the halo occupation approach is that it quantifies the bias of a class of galaxies with respect to the underlying dark matter distribution through the statistical relationship between galaxies and the dark matter halos in which they reside. In the HOD formalism, the bias of a galaxy sample is specified by the quantity  $P(N|M)$ , the probability that a halo of mass  $M$  contains  $N$  galaxies. Along with assumptions about the spatial and velocity biases of galaxies with respect to the dark matter within their host halos,  $P(N|M)$  describes the bias of the sample on all scales and for any clustering measure. The implicit assumption of this approach is that  $P(N|M)$  depends only the mass of the halo and is independent of the halo’s larger-scale environment. This “standard implementation” of the HOD has been called into question by a number of recent theoretical results. Thus it is important to test the underlying assumptions of the HOD and quantify any residuals of the standard implementation, reducing systematic uncertainties

in the cosmological constraints derived from HOD modeling. In turn these tests lead to insight on the processes of galaxy formation. In this paper we use new measurements of void probability statistics in the Sloan Digital Sky Survey (SDSS, York et al. 2000) and Two-Degree Field Galaxy Redshift Survey (2dFGRS, Colless et al. 2001, 2003) to test whether the relation between the properties of field galaxies and their host halos depends on mass only. We define field galaxies as isolated systems residing in low density regions of the galaxy distribution. In the halo occupation context, these are galaxies that live at the center of halos at or near the minimum halo mass scale for the given galaxy class.

In Tinker et al. (2006) (hereafter, Paper I), we demonstrated that the statistics of galaxy voids are a sensitive diagnostic for environmental dependence of halo occupation. The statistics explored in Paper I were the void probability function (VPF, denoted  $P_0$ ), and the underdensity probability function (UPF, denoted  $P_U$ ). The VPF is defined as the probability that a sphere of radius  $r$  contains zero galaxies of a given type. The UPF is defined as the probability that a sphere of radius  $r$  has a galaxy density less than some fraction of the overall mean density for that galaxy type. Here we set that fraction to the conventional value of 0.2. Previous theoretical studies sought to determine what information, if any, void statistics alone offer for constraining galaxy bias (Little & Weinberg 1994; Benson 2001; Berlind & Weinberg 2002). Paper I explored void statistics in conjunction with other clustering measures, demonstrating that standard HOD models that match observations of the projected two-point correlation function  $w_p(r_p)$ , and the number density of galaxies  $\bar{n}_g$ , predict nearly degenerate void statistics regardless of the mapping between halo

<sup>1</sup> Kavli Institute for Cosmological Physics, University of Chicago  
<sup>2</sup> Department of Astronomy & Astrophysics, University of Chicago  
<sup>3</sup> Department of Astrophysical Sciences, Princeton University  
<sup>4</sup> Institute for Astronomy, University of Edinburgh  
<sup>5</sup> Instituto de Astrofísica de Canarias  
<sup>6</sup> Department of Astronomy, Ohio State University  
<sup>7</sup> Theoretical Astrophysics, Los Alamos National Labs

mass and central galaxy luminosity or the amplitude of dark matter clustering, conclusions similar to those of Conroy et al. (2005). The remarkable robustness of void statistics (under the assumptions of the standard HOD) implies that they can be used to test these underlying assumptions. The two-point correlation function is dominated by galaxies in mean and high density regions of the universe. If one uses this statistic to constrain galaxy occupation and correctly predicts another clustering measure that probes underdense regions, then one infers that halo occupation at fixed mass does not change between high and low densities.

Early studies concluded that the properties of dark matter halos, such as their formation times and merger histories, were independent of, or weakly dependent on environment (Lemson & Kauffmann 1999; Sheth & Tormen 2004). More recent results, aided by higher resolution and larger-volume simulations, detect a clear relation between formation times and local environment (Gao et al. 2005; Harker et al. 2005; Wechsler et al. 2006; Zhu et al. 2006; Gao & White 2006; Wetzel et al. 2007). These studies conclude that this correlation is strongest for low-mass halos, with a sign such that older halos form in higher density regions. Attempts to measure this effect in high mass halos observationally have met with conflicting results (Yang et al. 2006; Berlind et al. 2006). Although the correlation between halo formation time and environment is now firmly established, the effect on the galaxy population is less clear. Croton et al. (2006b, 2007) use their semi-analytical galaxy formation model to quantify this “assembly bias” in the galaxy population. Croton et al. (2007) quantify assembly bias by its effect on the large-scale galaxy two-point correlation function,  $b_x = \sqrt{\xi/\xi_0}$ , where  $\xi_0$  is the clustering amplitude of a model once the assembly bias has been removed from the sample by scrambling galaxies among halos of the same mass. For luminosity-defined samples, they find  $b_x - 1 \approx 0.05$  for faint galaxies, decreasing to  $-0.05$  for bright galaxies. The effect is strongest in their model for faint, red, central galaxies, increasing the amplitude of the correlation function of these objects by nearly a factor of 4. Because central galaxies define the voids (in the statistical sense of the VPF and UPF), our approach is well-suited to testing this effect in the true galaxy distribution. Observational tests of the environmental dependence of galaxy properties by Blanton et al. (2006b) have shown that the blue fraction correlates with the galaxy density on small-scales (i.e., the scale of a large halo), but not with the larger-scale density field (see also Blanton et al. 2006a). Abbas & Sheth (2005, 2006) use the halo occupation formalism to calculate galaxy clustering as a function of local galaxy density, concluding that the standard  $P(N|M)$  approach correctly predicts the clustering of SDSS galaxies as a function of their local environment. Skibba et al. (2006) use the standard HOD approach to accurately predict the luminosity-weighted correlation function of SDSS galaxies. Our use of void statistics is complementary to these tests, in that voids probe the most extreme galaxy environments. While the papers above are sensitive to assembly bias of satellite galaxies or galaxies in mean and high-density environments, void statistics are affected by the bias of a small subset of the overall galaxy sample, making them more sensitive to assembly bias in central galaxies and at low densities.

In this paper we present new measurements of the VPF and UPF from Data Release Four of the SDSS (DR4, Adelman-McCarthy et al. 2006). Through the use of a larger observational sample, this work extends earlier analysis of

void statistics from the CfA redshift survey (Vogeley et al. 1994), the 2dFGRS (Croton et al. 2004; Hoyle & Vogeley 2004; Patiri et al. 2006) and Data Release Two of the SDSS (Conroy et al. 2005). We also present new measurements of the VPF from the full data release of the 2dFGRS that are better suited to the purposes of this study than earlier analyses. We compare these data to predictions for the VPF and UPF created with the standard implementation of the HOD and for models in which the occupation of central galaxies depends on environment. All models are constrained to match  $w_p(r_p)$  and  $\bar{n}_g$ . Using the parameterization of Paper I, we create density-dependent models in which the minimum mass scale for hosting a central galaxy shifts by a factor  $f_{\min}$  in environments where the density falls below a threshold value  $\delta_c$ . A value of  $f_{\min} > 1$  physically represents a model in which galaxy formation become less efficient in low-density regions, creating positive assembly bias ( $b_x > 1$ ). Models with  $f_{\min} < 1$  imply an increase in galaxy formation efficiency, in the sense that a given mass halo can host a more luminous galaxy, yielding negative assembly bias ( $b_x < 1$ ). We show that the void statistics for faint galaxies,  $M_r - 5 \log h < -19$ , are accurately predicted by the standard HOD, while models with density dependence always produce a worse fit to the observational data. The void statistics for bright galaxies,  $M_r - 5 \log h < -21$ , are adequately fit by the standard HOD prediction, while models with positive assembly bias are strongly excluded. (For reference, the characteristic luminosity  $L_*$  in the Blanton et al. (2003)  $r$ -band luminosity function is  $M_r - 5 \log h = -20.44$ .) We also make predictions for void statistics in the 2dFGRS. We find once again that the standard HOD accurately predicts the VPF in these samples, leaving little room for assembly bias.

We also explore models for faint color-defined galaxy samples. The dependence of galaxy color and morphology on local environment is well established (e.g. Dressler 1980; Postman & Geller 1984). The correlation between color and environment has been refined with the increased statistics of the SDSS, (Blanton et al. 2005a; Park et al. 2007). Berlind et al. (2005) use cosmological hydrodynamic simulations to demonstrate that these variations of color with environment can be explained by the variations of the halo mass function with environment only, without variations of halo occupation at fixed mass. The observational results of Blanton et al. (2006b) support this conclusion. However, the theoretical results of Croton et al. (2007) imply that environmental effects of halo occupation should be strong for color-defined samples. In their semi-analytic model, faint red central galaxies preferentially occupy halos in dense regions (at fixed halo mass). This is contrary to the standard HOD assumption that the central galaxy of a halo has a probability of being red that is independent of environment. We show that the measured VPFs are well-fit by the standard HOD predictions for these samples. An assembly bias as strong as that in the semi-analytic model of Croton et al. (2007) would likely be detectable within the given errors of our VPF measurements.

Section 2 presents the details of our measurements of the VPF and UPF from the SDSS, and our methodology for making predictions for these statistics from the HOD. Section 3 presents the results for luminosity-defined samples from the SDSS, comparing observational measurements to HOD predictions using both the standard implementation and models with density dependence. In §4 we show results for color-selected galaxy samples from the SDSS, and compare to HOD

models. In §5 we present results for luminosity-defined samples from the 2dFGRS. In §6 we discuss these results.

## 2. SDSS DATA AND MODELING

### 2.1. Observational Samples and Measurements

For SDSS galaxies, we use measurements of  $w_p(r_p)$  from Zehavi et al. (2005) (hereafter Z05). These measurements were performed on volume-limited samples from a spectroscopic sample of nearly 200,000 galaxies, from an angular survey area of 2497 deg<sup>2</sup>, approximately the size of Data Release Two of the SDSS (DR2, Abazajian et al. 2004). We use four volume-limited samples defined by  $r$ -band magnitude thresholds  $M_r - 5 \log h = -19, -20, -21, \text{ and } -22$ . For all samples, we utilize the full covariance error matrix of the measurements when comparing HOD models of  $w_p(r_p)$  to observations. To measure the void statistics in DR4 of the SDSS we use the NYU Value Added Galaxy Catalog (Blanton et al. 2005b). This sample is larger in volume than the Z05 sample; the survey area for DR4 is 4783 deg<sup>2</sup>, but the flanking fields and other isolated patches are not well suited for our measurements, and are not used. As in the Z05 samples, all galaxies are  $k$ -corrected to redshift  $z = 0.1$  using the software package `kcorrect` (Blanton & Rowles 2006). Although the larger volume of DR4 might lead to differences in  $w_p(r_p)$ , the samples for which  $w_p(r_p)$  have been measured in DR4 are within the errors of the Z05 data (I. Zehavi, private communication). As we will demonstrate in §2.3, the measurements of  $w_p(r_p)$  used in this paper are sufficient to constrain the HOD for the  $M_r - 5 \log h < -19$  and  $-21$  samples, so that the uncertainties in HOD parameters are nearly negligible in comparison to the measurement errors on the VPF and UPF. When analyzing the data we use the full error covariance matrix, also taken from Z05.

To measure the UPF and VPF from the survey at a given  $r$ , we randomly place a large number of spheres with radius  $r$  within the survey, counting the number of galaxies located in each sphere. We limit the number of spheres to a maximum of  $10^7$  and minimum of  $10^6$ , numbers that have been tested to ensure convergence. The largest number of spheres is used at small radii to reduce the shot noise in the measurement at those scales. Once the counts in each cell are determined, the VPF is defined as the fraction of empty spheres, i.e.,

$$P_0(r) = \frac{\mathcal{N}_0}{\mathcal{N}_{\text{tot}}}, \quad (1)$$

where  $\mathcal{N}_N$  refers to the number of spheres that contain  $N$  galaxies, and  $\mathcal{N}_{\text{tot}}$  indicates the total number of spheres. The UPF is defined as the fraction of spheres that contain less than 20% of the expected number of galaxies from the mean density,

$$P_U(r) = \mathcal{N}_{\text{tot}}^{-1} \sum_{N=0}^{N_U(r)} \mathcal{N}_N \quad (2)$$

where  $N_U(r) = \text{floor}(0.2 \times \bar{n}_g 4\pi r^3 / 3)$ . While  $P_0(r)$  rapidly approaches zero at radii larger than the mean galaxy separation,  $P_U(r)$  falls off approximately as an exponential function and is less subject to shot noise at larger  $r$ . Thus it is possible to measure  $P_U(r)$  more accurately at larger scales than  $P_0(r)$ . Paper I also demonstrated that these statistics have somewhat complementary information when testing for density-dependence in  $\langle N \rangle_M$ ; altering galaxy formation effi-

ciency may eliminate galaxies from low-density regions without entirely emptying them.

Our handling of the SDSS survey geometry and completeness closely parallels that of Conroy et al. (2005). The completeness, defined as the ratio of successfully attained redshifts to targetable objects, varies non-trivially from 0 to 1 as a function of right ascension and declination. Sophisticated software has been developed to efficiently handle complex survey geometry such as the SDSS. In order to identify and avoid regions of low completeness we use the `Mangle` package (Hamilton & Tegmark 2004) to generate a densely sampled angular window function. This window function incorporates regions of the sky not surveyed, either because the region lies outside the bounds of the survey or because of bright foreground stars, and incompleteness within the survey due either to fiber collisions (no two fibers can be separated by less than 55 arcseconds, affecting 7% of targetable redshifts) or objects that could not be assigned a reliable redshift, affecting  $\sim 1\%$  of targetable objects.

In order to treat edge-effects arising from measuring the VPF and UPF via counts-in-spheres, we convolve the window function with a circular smoothing kernel of angular radius  $\theta(r, z)$  proportional to a sphere projected onto the plane of the sky with comoving radius  $r$  at redshift  $z$ . This convolution yields the total completeness of the survey at each point in the sky for a given angular sphere size, where the incompleteness could arise from either a sphere lying partially off the edge of the survey or being in a region of the survey with low spectroscopic completeness. We then place random spheres only at points above a minimum convolved completeness. This allows us to robustly avoid regions of bright stars, regions of low completeness (due, for example, to inclement weather during observations) and the edges of the survey. The distribution of completenesses is approximately a Gaussian centered at  $\sim 88\%$  with an additional constant component extending to low completeness. Motivated by this distribution, we place spheres only in regions above a minimum convolved completeness of 83%, noting that our results are insensitive to this exact value. Spheres are placed uniformly along the line of sight because each sample is volume limited.

In the above methodology, completeness issues are handled by including only those regions of the survey which are both high and uniform in completeness and then incorporating the remaining small incompleteness effects into model predictions (which we will discuss below). An alternative methodology has been proposed by Croton et al. (2004), in which incompleteness effects are treated by correcting the measured VPF in order to recover the “true” underlying VPF of the galaxy distribution. This particular correction scheme counts the number of galaxies within a sphere of radius  $r' = r/f^{1/3}$  as contributing to the VPF at radius  $r$  ( $f$  is the convolved completeness at  $r$ ). This scheme in essence treats incompleteness as missed volume rather than missed galaxies. Although this correction is exact in the Poisson limit, it will over-correct the VPF to some degree at larger  $r$  or lower  $P_0(r)$ . The systematic error accrued is difficult to estimate without the use of detailed mock catalogs, reducing the usefulness of the correction method in the first place. Thus to compare our models to data, we modify the theoretical predictions to match the incompleteness of the survey, rather than trying to remove the incompleteness from the survey itself. We will discuss this further in §2.3.

As in Z05, we create two separate volume-limited samples

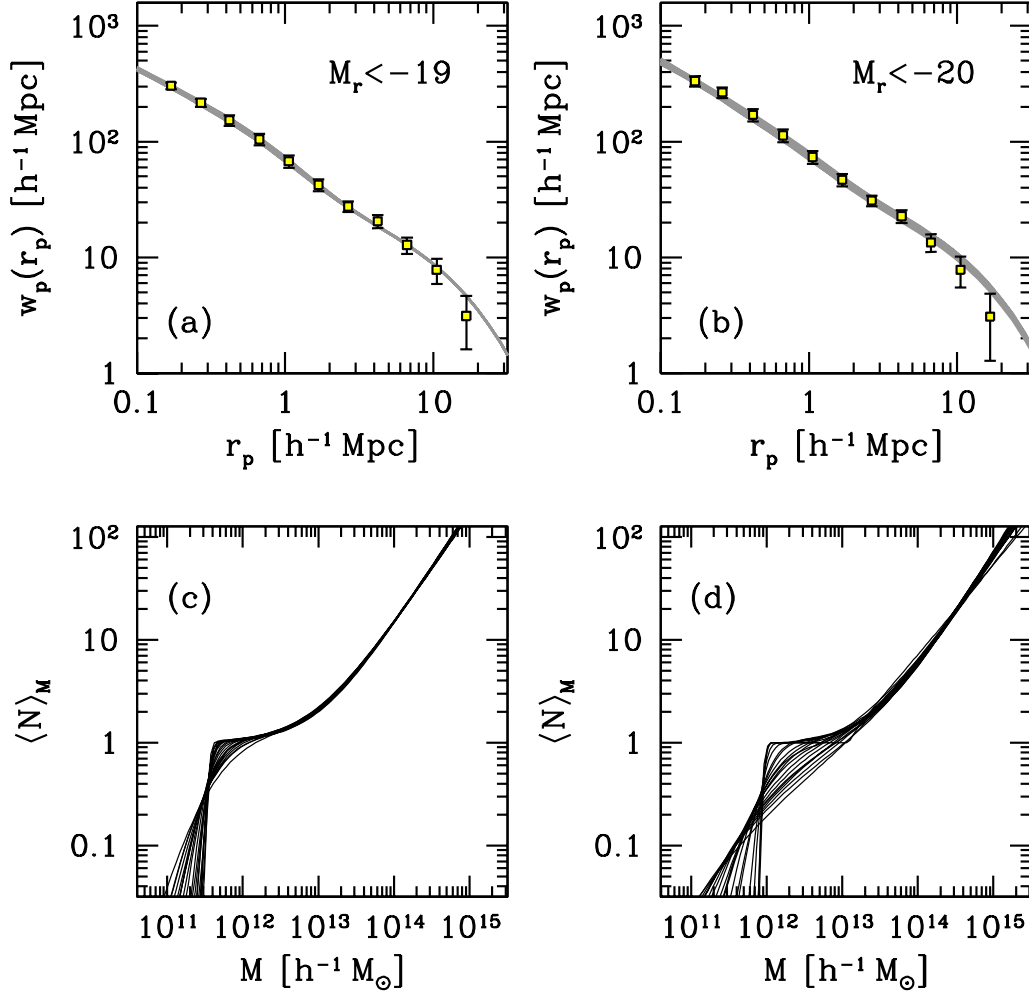


FIG. 1.— Projected correlation function data and HOD fits for the  $M_r - 5 \log h < -19$  sample (panels [a] and [c], respectively) and the  $M_r - 5 \log h < -20$  sample (panels [b] and [d], respectively). In the top panels, points with error bars are the SDSS data of Z05, while the gray region represents the range in HOD fits with  $\Delta\chi_{w_p}^2 < 1$  with respect to the best-fit HOD model. Bottom panels plot the mean occupation functions  $\langle N \rangle_M$  for 20 randomly chosen HOD fits with  $\Delta\chi_{w_p}^2 < 1$ . Results in panels (b) and (d) are for the  $M_r - 5 \log h < -20$  sample restricted to  $z \leq 0.06$ .

TABLE 1  
PROPERTIES OF THE SDSS VOLUME LIMITED CATALOGS

Sample	$z_{\min}$	$z_{\max}$	$\bar{n}_g$	$f_{\text{comp}}$	Volume [ $(h^{-1} \text{Mpc})^3$ ]
-19	0.02	0.06	$1.19 \times 10^{-2}$	0.873	$1.78 \times 10^6$
-20	0.02	0.06	$4.33 \times 10^{-3}$	0.873	$1.78 \times 10^6$
-20'	0.02	0.10	$4.93 \times 10^{-3}$	0.873	$8.28 \times 10^6$
-21	0.03	0.15	$1.01 \times 10^{-3}$	0.876	$2.11 \times 10^7$
-22	0.05	0.22	$5.77 \times 10^{-5}$	0.876	$8.15 \times 10^7$
red	0.02	0.06	$3.28 \times 10^{-3}$	0.873	$1.78 \times 10^6$
blue	0.02	0.06	$4.33 \times 10^{-3}$	0.873	$1.78 \times 10^6$

NOTE. — Number densities are given in units of  $(h^{-1} \text{Mpc})^3$ .  $f_{\text{comp}}$  is the mean completeness of each sample. -20' refers to the unrestricted sample that includes the Sloan Great Wall. See §2.2 for discussion.  $V$  is the volume of each sample. Samples are defined with luminosity thresholds, but the red and blue samples are restricted to the magnitude range  $-19 < M_r - 5 \log h < -20$ .

with  $M_r - 5 \log h < -20$ . The maximum redshift for these objects is  $z = 0.10$ , but this redshift limit includes the so-called ‘Sloan Great Wall’ supercluster (Gott et al. 2005; see also Baugh et al. 2004 for results from the 2dFGRS). This struc-

ture dominates the overall clustering of the full -20 sample, and the presence of such a structure makes it difficult to accurately estimate the true cosmic variance for this sample. We follow Z05 in focusing on a sample restricted to the same

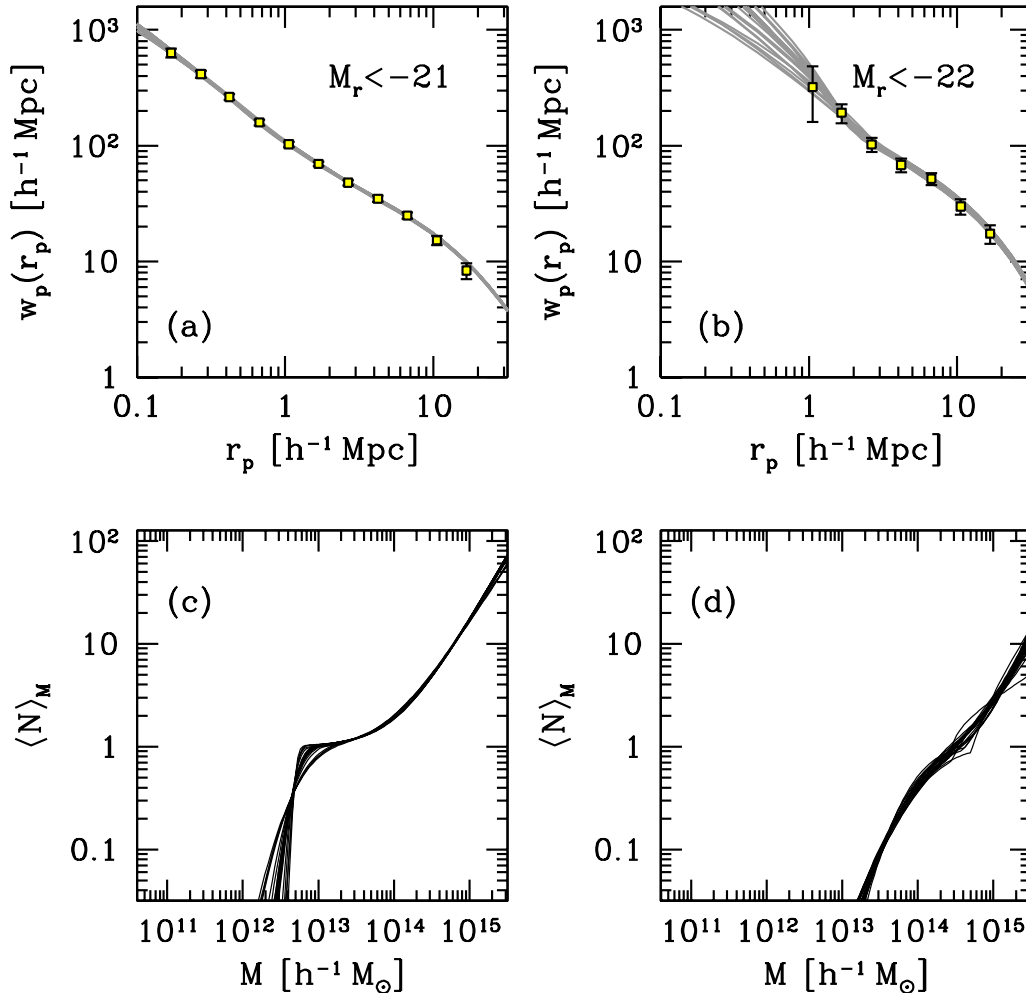


FIG. 2.— Projected correlation function data and HOD fits for the  $M_r < -21$  sample (panels [a] and [c], respectively) and the  $M_r < -22$  sample (panels [b] and [d], respectively). In the top panels, points with error bars are the SDSS data of Z05, while the gray region represents the range in HOD fits with  $\Delta\chi^2_{w_p} < 1$  with respect to the best-fit HOD model. Bottom panels plot the mean occupation functions  $\langle N \rangle_M$  for 20 randomly chosen HOD fits with  $\Delta\chi^2_{w_p} < 1$ .

redshift limit as the  $M_r - 5 \log h < -19$  sample of  $z \leq 0.06$ . Unless otherwise stated, all results for these galaxies use the restricted redshift sample.

## 2.2. HOD Modeling

We constrain the occupation function by fitting the observed  $w_p(r_p)$  and  $\bar{n}_g$  for each sample with the analytic model for  $w_p(r_p)$  described in Tinker et al. (2005) (see also Zheng 2004; Zehavi et al. 2004). The mean occupation function is divided into two terms; central galaxies located at the center of mass of the halo, and satellite galaxies distributed throughout the halo. For SDSS samples defined by a luminosity threshold, the central occupation function takes the form

$$\langle N_{\text{cen}} \rangle_M = \frac{1}{2} \left[ 1 + \text{erf} \left( \frac{\log M - \log M_{\text{min}}}{\sigma_{\log M}} \right) \right], \quad (3)$$

where  $M_{\text{min}}$  is a cutoff mass scale and all logarithms are base-10. Formally, in equation (3)  $M_{\text{min}}$  is the mass at which  $\langle N_{\text{cen}} \rangle_M = 0.5$ . The parameter  $\sigma_{\log M}$  describes the shape of the central galaxy cutoff. Physically, this parameter represents the scatter between halo mass and central galaxy luminosity;

if this scatter is large then a fraction of low-mass halos will be included in the sample and the shape of the cutoff will be soft. If this scatter is small then central galaxies follow a nearly one-to-one mapping of mass to luminosity, and  $\langle N_{\text{cen}} \rangle_M$  resembles a step function.

The satellite galaxy occupation function is modeled as a truncated power law,

$$\langle N_{\text{sat}} \rangle_M = \left( \frac{M - M_{\text{cut}}}{M_{\text{sat}}} \right)^{\alpha_{\text{sat}}}, \quad (4)$$

where  $M_{\text{cut}}$  is a cutoff mass scale for satellites,  $M_{\text{sat}}$  is the amplitude of the power law, and  $\alpha_{\text{sat}}$  is its slope. In equation (4) the mass at which halos host on average one satellite is  $M_1 = M_{\text{cut}} + M_{\text{sat}}$ . The total occupation function is  $\langle N \rangle_M = \langle N_{\text{cen}} \rangle_M + \langle N_{\text{sat}} \rangle_M$ . As expressed in equations (3) and (4) the occupation function has five free parameters. In practice, the number of free parameters is reduced to four because  $M_{\text{min}}$  is set by  $\bar{n}_g$  once the other parameters have been chosen. One can accurately fit  $w_p(r_p)$  with only a three-parameter occupation function (e.g., Zehavi et al. 2004, 2005), but we allow  $\langle N \rangle_M$  extra freedom to explore how variations in the

shape of  $\langle N \rangle_M$  alter the predicted void statistics. In Paper I we demonstrated that the void statistics are relatively insensitive to  $\sigma_{\log M}$  and  $M_{\min}$  allowed by  $w_p(r_p)$  and  $\bar{n}_g$ , but to quantify the uncertainty in our predicted void statistics we leave all parameters free. For each  $w_p(r_p)$ , the best-fit model is found by  $\chi^2$  minimization using the full covariance error matrix of the data. To minimize  $\chi^2$  we use the Monte Carlo Markov chain method (MCMC). While less efficient than other techniques, MCMC quantifies the errors on the HOD parameters. For each sample, we randomly select twenty HOD fits from the MCMC chain that have a  $\Delta\chi^2 < 1$  with respect to the best-fit model. These 20 fits will be used to estimate the range in HOD predictions for the void statistics allowed by the  $w_p(r_p)$  data. The best-fit models for each sample are listed in Table 2.

Figure 1 presents the results of the HOD analysis of the  $M_r - 5 \log h < -19$  and  $-20$  samples. Figures 1a and 1b plot the data with diagonal error bars, along with the sample of twenty HOD fits from the MCMC chain. Figures 1c and 1d present the occupation functions for each of those twenty fits for faint and bright samples, respectively. For the  $M_r - 5 \log h < -19$  sample, the twenty projected correlation functions calculated from the HOD fits are nearly indistinguishable. But the occupation functions in 1c differ substantially at low masses. Because  $M_{\min}$  for this sample is significantly below the non-linear mass scale  $M_* = 8.60 \times 10^{12} h^{-1} M_\odot$  for this cosmology,  $w_p(r_p)$  is relatively unaffected by softer or harder central cutoffs; the mean bias of the HOD is largely unaffected by variations in  $\sigma_{\log M}$ . In Paper I we demonstrated that the distribution of voids is also unaffected by such changes to the occupation function, yielding degenerate VPFs and UPFs. Figure 1d presents the twenty occupation function for the  $M_r - 5 \log h < -20$  sample. For this sample, the shape of the central galaxy cutoff is essentially unconstrained; the range in  $\sigma_{\log M}$  from the twenty MCMC models is 1.4 to 0.05. Because the volume of this sample is the same as the  $M_r - 5 \log h < -19$  sample, the differences in the constraints are somewhat surprising. The size of the diagonal errors on  $w_p(r_p)$  are similar, but the data points for the brighter galaxies are more correlated, reducing the constraining power for this sample.

Figure 2 shows the same quantities as the previous figure, but now for the  $M_r - 5 \log h < -21$  sample, and the  $M_r - 5 \log h < -22$  sample. Figure 1c presents the twenty occupation functions for the  $M_r - 5 \log h < -21$  sample. For this sample,  $M_{\min} \sim M_*$ , thus the constraints on  $\sigma_{\log M}$  from  $w_p(r_p)$  alone are substantially stronger than for the fainter samples. For the brightest galaxies, Figure 2b shows large differences in one-halo clustering among acceptable models, resulting in significant differences in  $\langle N_{\text{sat}} \rangle_M$  in Figure 2d. The lack of strong constraints on the HOD prevent the use of this sample and the  $M_r - 5 \log h < -20$  sample for testing assembly bias in the void statistics. But, as we will show in the following section, for these the constraints on the HOD can be enhanced moderately through the addition of the VPF and UPF.

### 2.3. Mock Catalogs

Once the best-fit HOD model is identified, we predict void statistics by populating the halos identified in dark matter N-body simulations. Central galaxies are located at the center of mass of the halo, and satellite galaxies are placed randomly throughout the halo such that they follow the density profile of Navarro et al. (1997) with a concentration parameter given by the model of Bullock et al. (2001). Central galaxies are given the velocity of the halo center of mass, while satellite galax-

ies are given an additional random velocity in each Cartesian direction drawn from a Gaussian distribution with dispersion equal to the virial velocity of the halo  $\sigma_{\text{vir}}^2 = GM/2R_{\text{vir}}$ , where we have defined  $R_{\text{vir}}$  to be the radius at which the mean interior density of the halo is 200 times the background density. All calculations of the VPF and UPF are performed in redshift space using the distant observer approximation, with the  $z$ -axis as the line of sight. Our results are insensitive to the value of  $\Omega_m$  or possible velocity bias of the galaxies within reasonable limits (i.e., variations less than  $\sim 40\%$ ). Although these parameters alter the redshift space positions of galaxies, the net effect on the void statistics is negligible. As with the observational measurements, we calculate the VPF and UPF using  $10^6 - 10^7$  random spheres at each radius. Errors on the calculations are estimated by jackknife sampling of the simulation volume into 125 subsamples.

We use two simulations to calculate void statistics, a smaller box  $400 h^{-1} \text{Mpc}$  on a side and a larger box  $1086 h^{-1} \text{Mpc}$  on a side. Both simulations are inflationary cold dark matter models with identical cosmologies. The linear matter power spectrum used to create the initial conditions of each simulation was calculated with CMBFAST (Seljak & Zaldarriaga 1996) with the parameter set  $(\Omega_m, \sigma_8, \Omega_b, n_s, h) = (0.3, 0.9, 0.04, 1.0, 0.7)$ . For fainter galaxies we utilize the smaller simulation to make predictions. This is the same simulation used in Paper I, consisting of  $1280^3$  particles, yielding a particle mass of  $2.54 \times 10^9 h^{-1} M_\odot$ . To model the brighter galaxies we populate the larger simulation. This simulation contains  $1024^3$  particles, yielding a particle mass of  $9.95 \times 10^{10} h^{-1} M_\odot$ . For both simulations, the initial conditions are integrated with the hashed oct-tree code of Warren & Salmon (1993), with Plummer force softening lengths of  $14.6 h^{-1} \text{kpc}$  and  $40 h^{-1} \text{kpc}$  for the small and large boxes, respectively. Halos are identified in the simulations using the friends-of-friends algorithm with a linking parameter of 0.2 times the mean interparticle separation, a value that selects halos roughly corresponding to our adopted definition of a virial overdensity of 200 (Davis et al. 1985). To be self-consistent, all analytic calculations are performed with the same set of cosmological parameters listed above. For these calculations, the halo mass function is obtained with the fitting function of Jenkins et al. (2001). For the halo bias function, we use the fitting function from Tinker et al. (2005). This bias relation utilizes the functional form presented in Sheth et al. (2001), but with parameter values ( $a = 0.707$ ,  $b = 0.35$  and  $c = 0.8$ ) calibrated on a set of larger-volume N-body simulation with widely varying cosmologies.

As mentioned in §2.1, we modify the number density of galaxies in each mock to match that measured in each observational sample. At each radius the mean number density of SDSS galaxies within spheres  $\bar{n}_g(r)$  is calculated. The maximum deviation of  $\bar{n}_g(r)$  from the overall mean averaged over all radial bins in less than  $\sim 2\%$  for each luminosity sample, demonstrating that our treatment of the survey mask is robust and that we are probing the same volume with each sphere size. The mean number densities for each sample are listed in Table 1, along with other details of each sample. Due to incompleteness, these number densities are less than that expected from the measurement of the  $r$ -band luminosity function by Blanton et al. (2003). When calculating the VPF in our mock galaxy distributions, we dilute the mocks to match the number densities of the data at each radius. Using the overall mean density produces minimal differences in the theoretical predictions, with small differences at the lowest- $r$

points where the VPF is Poisson dominated.

The galaxy number density required by the HOD analysis of  $w_p(r_p)$  is the *true* number density, which must be estimated from observational samples and has an error associated with it due to cosmic variance. As noted in Abazajian et al. (2005), this error is  $\lesssim 5\%$  for the  $M_r - 5 \log h < -21$  sample. To test the sensitivity of our model predictions to errors in the true number density, we alter  $\bar{n}_g$  by  $\pm 10\%$  and re-fit  $w_p(r_p)$ . The resulting void statistics, once matched to the *sample* number densities, are within the errors on the theoretical estimates. Due to the steepness of the halo mass function, increasing or decreasing  $\bar{n}_g$  by 10% alters the mass scales of the HOD parameters ( $M_{\min}$ ,  $M_1$ ,  $M_{\text{cut}}$ ) by  $\sim 5\%$  (with the opposite sign of the change in  $\bar{n}_g$ ), but the overall shape of the HOD is nearly unchanged. We conclude that cosmic variance errors on the true galaxy number density do not bias our results.

#### 2.4. Error Estimation and Systematics

We estimate the errors on the measured void statistics with our simulations, described the previous section. The volume of the  $M_r - 5 \log h < -19$  and  $-20$  samples is approximately equal to a cube  $120 h^{-1} \text{Mpc}$  per side,  $1/37$  the volume of the  $400 h^{-1} \text{Mpc}$  box. Once the HOD predictions have been calculated, using the best-fit HOD from the  $w_p(r_p)$  fitting, the box is divided into 27 cubic subregions, each  $133 h^{-1} \text{Mpc}$  per side. The dispersion among the subregions is scaled by  $(133/120)^{3/2} = 1.17$  to correct for the fact that the subregions do not exactly match the volume of the observational sample. This scaled dispersion is taken to be the error on the observational quantity. We also estimate the covariance matrix from this method. This method is more robust than estimating the errors directly from the observational sample due to variations of the galaxy number density on  $120 h^{-1} \text{Mpc}$  scales. When estimated directly from the data, these fluctuations cause the errors to be underestimated with respect to the dispersion amongst the simulation subregions. At large scales,  $r \sim 10 h^{-1} \text{Mpc}$  in the fainter samples, proper error estimation from the data is also inhibited by small sample volume. To estimate errors for the brighter samples, the same process is followed using the  $1086 h^{-1} \text{Mpc}$  box. For the  $M_r - 5 \log h < -21$  sample, this larger simulation is approximately 47 times larger. For  $M_r - 5 \log h < -22$  galaxies, the volume of the large simulation is equivalent to 16 times the observational sample. When calculating  $\chi^2$  for a given model, we neglect the innermost ( $r = 1 h^{-1} \text{Mpc}$ ) data point. In tests we find that the errors on this scale require a prohibitive number of random spheres to converge, and including this point in the covariance matrix introduces significant noise to the error estimate. The data at this scale contain little useful information anyway; the behavior of the VPF is nearly Poisson at  $r \lesssim 1 h^{-1} \text{Mpc}$  for all luminosity samples (Croton et al. 2004).

For clarity, we will refer to  $\chi^2$  values with respect to  $P_0(r)$ ,  $P_U(r)$ , and  $w_p(r_p)$  as  $\chi_{\text{VPF}}^2$ ,  $\chi_{\text{UPF}}^2$ , and  $\chi_{w_p}^2$ , respectively.

### 3. RESULTS FOR LUMINOSITY-DEFINED SDSS SAMPLES

#### 3.1. Observational Results and HOD Predictions

Our approach is to take a random sample of 20 HOD models that all produce accurate fits to the  $w_p(r_p)$  data, and for each model calculate the VPF and UPF. All HOD models are  $\Delta\chi_{w_p}^2 < 1$  with respect to the best-fitting model. As shown in Table 1, the best-fit models all yield  $\chi_{w_p}^2/\nu \lesssim 1$ . Conroy et al. (2005) and Paper I concluded that  $P_0(r)$  contained little additional information about the galaxy distribution relative to

the two-point correlation function. If this is exactly true, and the precision of the measurements of the different statistics are equal, we would expect that 1) all 20 models will produce good fits to the void statistics, and 2) that the range in  $\chi_{\text{VPF}}^2$  will be approximately 1, just as with the distribution of  $\chi_{w_p}^2$  values. If the void statistics do contain complementary information about the galaxy distribution, one or both of these expectations will be violated. An alternate method would be to perform a joint fit to  $w_p(r_p)$ ,  $P_0(r)$ , and  $P_U(r)$  simultaneously, and then compare the constraints on HOD parameters to the analysis in which  $w_p(r_p)$  is considered alone. Because calculating the void statistics involves the use of an N-body simulation this procedure is time intensive. It also requires an estimate of the covariance between all three data sets, which is not available. This method is more rigorous than the one we employ, but our approach provides a straightforward test of the HOD models, and discrepancies between predictions and measurements are readily detectable and quantifiable.

Figure 3 plots the measured SDSS VPF for the four luminosity samples in Table 1 and compares them to the best-fit models using the standard implementation of the HOD. In each panel, the points with error bars represent the observed SDSS values. Lines show the VPF obtained from the populated simulations. The lower panels in each quadrant present the residuals of the model from the data. We define the residual as  $\Delta P/\sigma_{\text{SDSS}} \equiv (P_0^{\text{HOD}} - P_0^{\text{SDSS}})/\sigma_{\text{SDSS}}$ , where  $\sigma_{\text{SDSS}}$  is the diagonal error bar on the SDSS data. We divide by the error to more clearly present the differences between theory and observations; the fractional error on the VPF (and the UPF) can range from  $10^{-3}$  at small radii to  $\sim 1$  at large  $r$ . The data are highly correlated, so a  $\Delta P/\sigma_{\text{SDSS}} \sim 1$  for several consecutive data points is still only a  $\sim 1\sigma$  deviation overall. The errors on the lines are the jackknife error bars, quantifying the theoretical uncertainty in our predicted VPF for the HOD model that best fits  $w_p(r_p)$ , resulting from the finite volume of the simulation. The shaded region in the lower window of each panel represents the range in  $P_0(r)$  from the MCMC models, quantifying the uncertainty in the theoretical prediction associated with the uncertainty in the HOD parameters. We now describe each sample in detail.

Figure 3a presents the results for the  $M_r - 5 \log h < -19$  sample. Due to the low luminosity threshold, this sample has the smallest volume and largest observational errors on both  $w_p(r_p)$  and the void statistics. It also has the highest number density, driving the VPF to zero at the smallest value of  $r$  of all four samples. The agreement between the measured VPF and that predicted by the best-fit HOD, which assumes no density dependence to  $\langle N \rangle_M$ , is excellent. The residuals are approximately  $0.5\sigma_{\text{SDSS}}$  or less at all  $r$ . The  $\chi_{\text{VPF}}^2$  for the best-fit model is 8.99 for 10 data points (note that “best-fit” here refers to  $w_p(r_p)$ , and no parameters are adjusted to match the VPF itself). Due to the errors on  $w_p(r_p)$ , the range in predicted  $P_0(r)$  from the set of acceptable HOD fits is larger than the jackknife errors on  $P_0(r)$  for an individual model, but  $\Delta P/\sigma_{\text{SDSS}} \lesssim 1$  for all HOD models with  $w_p(r_p)$  fits of  $\Delta\chi_{w_p}^2 < 1$ . The  $\chi_{\text{VPF}}^2$  values for these models range from 8.27 to 11.7. We attribute the larger range of  $\chi_{\text{VPF}}^2$  of 3.4 mostly to the increased volume of the DR4 sample relative to the  $w_p(r_p)$  sample.

Figure 3b presents the results for  $M_r - 5 \log h < -20$  galaxies. The points with error bars in the upper panel of Figure 3b show the results from the restricted sample. The best-fit HOD prediction is  $\sim 2\sigma$  low at  $r \geq 4 h^{-1} \text{Mpc}$ , yielding  $\chi_{\text{VPF}}^2 = 54.2$  for 10 data points. The range in  $\chi_{\text{VPF}}^2$  from the twenty MCMC

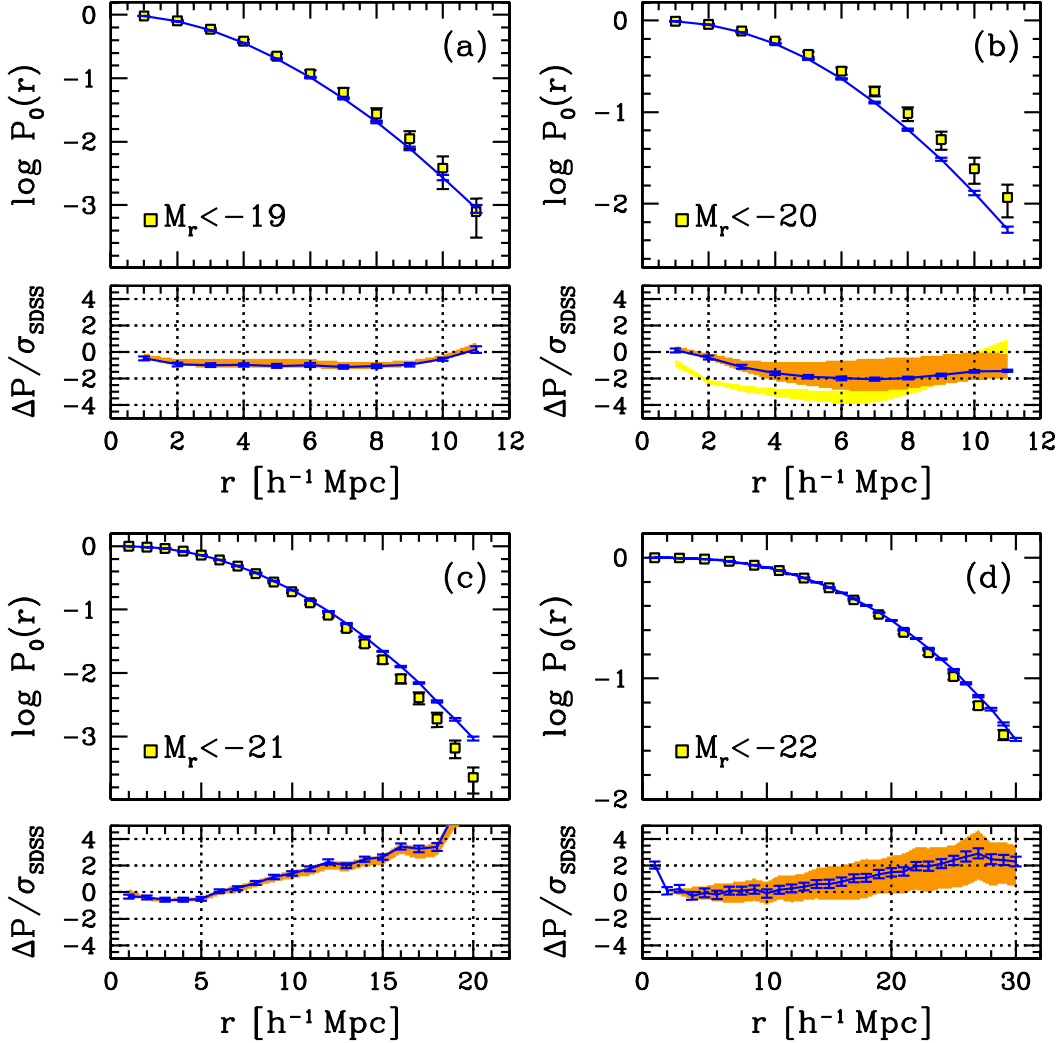


FIG. 3.— Comparison of the measured SDSS VPF to HOD predictions from fitting  $w_p(r_p)$ . The luminosity sample is labeled in each panel. The results for each sample are presented in two panels; the upper panel presents the SDSS  $P_0(r)$  and the HOD prediction, while the lower panel plots difference between the data and prediction, relative to the errorbar on the data. The errors on the HOD prediction are calculated from the simulation by the jackknife method. The shaded region in the lower panel represents the range in predictions from a sample of HODs with  $\Delta\chi^2_{w_p} < 1$  with respect to the best-fit model. The data and model in the  $M_r < -20$  panels are using the restricted volume-limited sample. The yellow shaded region plots the results from using the full sample,  $z \leq 0.10$ .

models is 11.4 to 118. This is in sharp contrast to the results in 3a, in which a set of  $w_p(r_p)$  models with  $\Delta\chi^2_{w_p} \leq 1$  produces a set of VPFs with  $\Delta\chi^2_{\text{VPF}} \leq 4$ . This is due to the large range in  $\sigma_{\log M}$  allowed by the  $w_p(r_p)$  data. Although the VPF is most sensitive to the fraction of galaxies that are satellites, large variations in the central occupation function still influence the size of voids to some degree (Paper I, Figure 6). The value of  $\chi^2_{\text{VPF}}$  correlates with the  $\sigma_{\log M}$  such that sharper central cutoffs yield more accurate predictions for  $P_0(r)$ , with a correlation coefficient  $r = 0.94$ . Combined with the fact that the central cutoff shape is ill-constrained by  $w_p(r_p)$  alone, the VPF adds significant information for constraining the HOD for this sample; models with  $\sigma_{\log M} < 0.3$  yield  $\chi^2_{\text{VPF}} \lesssim 12$ . The yellow shaded region presents the residuals for VPF predictions for the same analysis as the orange shaded region, but now using the full  $z \leq 0.10$  volume. The larger volume and smaller  $w_p(r_p)$  errors tighten the constraints on the HOD, but as noted in Z05 the presence of the Sloan Great Wall makes it difficult to find an HOD model that accurately fits the am-

plitude of the correlation function in the two-halo regime. The supercluster boosts the large-scale power in the two-point clustering, and dramatically alters the three-point clustering (Nichol et al. 2006; Baugh et al. 2004; Gaztañaga et al. 2005). This amplification of clustering creates larger voids in the galaxy distribution, producing residuals with respect to the HOD predictions that are significantly negative.

Figure 3c presents the results for the  $M_r - 5 \log h < -21$  sample. Although this sample includes the Sloan Great Wall, the volume of this sample is large enough such that the inclusion of this structure does not significantly alter the clustering statistics. Recall that for this sample (and for the  $M_r - 5 \log h < -22$  sample), we use the  $1086 h^{-1} \text{Mpc}$  box to calculate the HOD predictions and estimate the observational errors. The residuals of the best-fit model are  $\Delta P / \sigma_{\text{SDSS}} \lesssim 1$  for  $r < 10 h^{-1} \text{Mpc}$ , but at larger scales the residuals gradually increase to the point where the residuals between the best-fit model and data are  $\sim 2\sigma_{\text{SDSS}}$  at  $r > 12 h^{-1} \text{Mpc}$ . The  $\chi^2_{\text{VPF}}$  for the best-fit model prediction is 27.1 for 19 data points. The range of  $\chi^2_{\text{VPF}}$  values for the MCMC sample of models

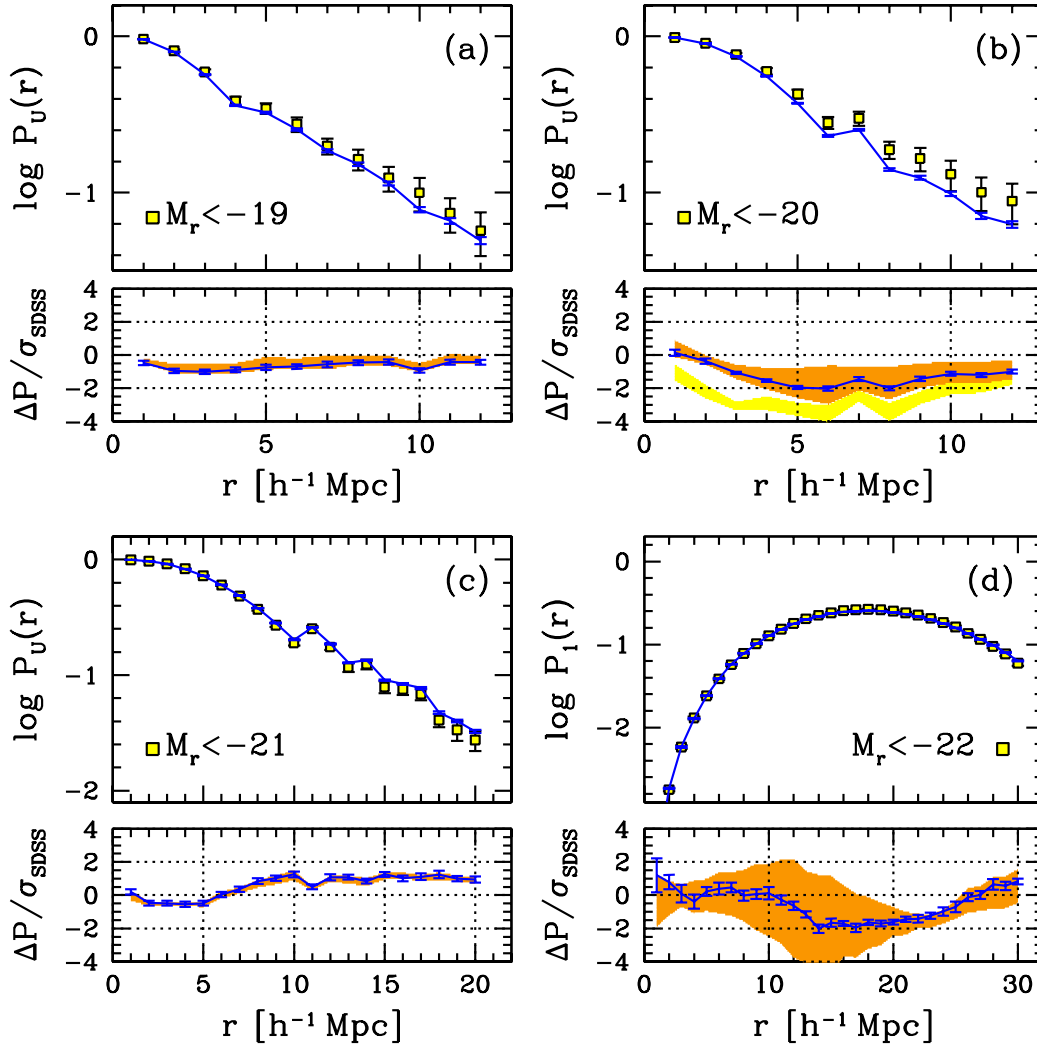


FIG. 4.— Comparison of the measured SDSS UPF to HOD predictions from fitting  $w_p(r_p)$ . Jumps in the predictions and data occur when the number of galaxies corresponding to 20% of the mean density crosses an integer boundary in the number of galaxies required to make a sphere “underdense”. For the  $M_r < -22$  sample, the number density is so low that the UPF only differs from the VPF at  $r > 26 h^{-1} \text{ Mpc}$ , so we have plotted  $P_1(r)$  instead. As in Figure 3, the  $M_r < -20$  panels have an additional yellow shaded region comparing the  $P_0(r)$  from the  $z \leq 0.10$  sample with the HOD constraints from  $w_p(r_p)$  for the same sample.

is  $\chi_{\text{VPF}}^2 = 22.1$  to  $\chi_{\text{VPF}}^2 = 29.2$ , indicating that  $P_0(r)$  adds some complementary information to  $w_p(r_p)$  for constraining the occupation function, assuming that the HOD is environment independent. The value of  $\chi_{\text{VPF}}^2$  is negatively correlated with  $\sigma_{\log M}$ , but the correlation is much weaker than in Figure 3b, with a correlation coefficient  $r = -0.59$ . For this model, a joint fit to both  $w_p(r_p)$  and  $P_0(r)$  would most likely find a solution with a combined  $\chi^2/\nu < 1$ . We will discuss this further in the following section.

Figure 3d presents the results for  $M_r - 5 \log h < -22$  galaxies. This sample has the largest volume, but galaxies above this magnitude threshold are rare. Thus Poisson fluctuations contribute substantially to the jackknife errors on  $w_p(r_p)$  at smaller scales, and the Z05  $w_p(r_p)$  for this sample has no pairs at  $r_p < 1 h^{-1} \text{ Mpc}$ . The lack of information on clustering in the one-halo regime decreases the constraints that can be placed on the HOD. The best-fit HOD model is in good agreement with the observations, with  $\chi_{\text{VPF}}^2 = 29.0$  for 29 data points. The range of  $\chi_{\text{VPF}}^2$  for the MCMC models is large, extending

from 23.4 to 52.0. The shape of the central cutoff for these models varies from  $\sigma_{\log M} = 0.5$  to  $\sigma_{\log M} = 0.8$ . The halos that contain galaxies in this magnitude regime lie in the exponential cutoff of the mass function, where the halo bias is a strong function of mass. Models with higher values of  $\sigma_{\log M}$  have on average lower  $\chi_{\text{VPF}}^2$  values with respect to the VPF, yielding  $r = -0.74$ . Thus for samples of objects with limited clustering information at small scales, extra constraining power can be obtained through void statistics.

Figures 4a–4c present the UPF results for the same four luminosity samples. In each figure the upper panel shows the measured UPF for SDSS galaxies and the best-fit HOD prediction. As in Figure 3, the lower panels plot the residuals between data and best-fit model, as well as the range in predictions from the 20 MCMC models. The comparison of this statistic to the HOD predictions are similar to those of the VPF. In Figure 4a, the  $\chi_{\text{UPF}}^2$  for the best-fit model is 9.93 for 11 data points, with a range of 7.17 to 11.7 for the MCMC models. In Figure 4b, the best-fit HOD model is once again  $\sim 2 - \sigma$  below the observations at  $r \geq 4 h^{-1} \text{ Mpc}$ , yield-

ing  $\chi_{\text{UPF}}^2 = 69.8$  for 11 data points. The range in  $\chi_{\text{UPF}}^2$  values is 10.7 to 93.9, with  $\chi_{\text{UPF}}^2$  correlating with the value of  $\sigma_{\log M}$  as with the models in Figure 3b. In Figure 4c, the HOD predictions are in better agreement with the data at large scales than the VPF results from 3c, yielding  $\chi_{\text{UPF}}^2 = 20.7$  for 19 data points. The range of  $\chi_{\text{UPF}}^2$  values from the MCMC models is smaller than the VPF results, with maximum and minimum  $\chi^2$  values of 22.0 and 16.5, respectively.

For  $M_r - 5 \log h < -22$  galaxies, the UPF contains little new information with respect to the VPF. The number density of this sample is low enough that a single galaxy in a sphere is enough to make the local density larger than the threshold of  $0.2\bar{n}_g$  for all  $r < 27 h^{-1} \text{Mpc}$ . Therefore we compare predictions and measurements for  $P_1(r)$ , the probability that a random sphere has exactly one galaxy within it. For  $r < 16 h^{-1} \text{Mpc}$  this statistic probes overdense regions ( $\delta_g > 0$ ). At large and small scales, the agreement between the data and best-fit model are excellent. At intermediate scales,  $8 < r < 18 h^{-1} \text{Mpc}$ , the agreement is adequate but the range of predictions is wide, resulting from the lack of tight constraints on the HOD from  $w_p(r_p)$  alone.

With the exception of the  $M_r - 5 \log h < -20$  sample, void statistics do not provide a significant amount of new information about HOD parameters, but for each sample they do tighten the constraints on the shape of the central galaxy cut-off parameter,  $\sigma_{\log M}$ , relative to  $w_p(r_p)$  alone.

### 3.2. Comparison to Density-Dependent Models

In Paper I we presented a simple model for density-dependent occupation functions that focuses on changes to the minimum mass scale for central galaxies. The parameters of this model are  $\delta_c$ , the threshold density below which the HOD changes, and  $f_{\min}$ , the factor by which  $M_{\min}$  changes in these low density regions. We calculate the local density of each halo with a top-hat smoothing filter with radius  $5 h^{-1} \text{Mpc}$ . For example, if  $\delta_c = -0.5$  and  $f_{\min} = 2$ , halos in regions that are below 50% of the cosmic mean density must be twice as massive (relative to halos in denser regions) in order to host a galaxies above the luminosity threshold. A value of  $f_{\min} = \infty$  corresponds to complete suppression of galaxies in regions below  $\delta_c$ . We can place these models in the context of assembly bias as defined by Croton et al. (2007) by calculating the ratio of the large-scale correlation function in the density-dependent model to its standard counterpart, i.e.,  $b_x = \sqrt{\xi/\xi_0}$ . We find that  $b_x \gtrsim 5\%$  for  $\delta_c \gtrsim -0.5$  and  $f_{\min} > 2$  for models of the  $M_r - 5 \log h < -19$  sample. For the brighter sample,  $b_x \gtrsim 5\%$  for models with  $\delta_c \gtrsim -0.1$ . We demonstrated in §3.1 that the  $M_r - 5 \log h < -19$  and  $-21$  void statistics are already well-fit by the standard HOD. Thus adding two new parameters will not statistically improve the model. But we explore density dependent models in order to constrain the level of assembly bias for central galaxies: to what degree can  $f_{\min}$  differ from unity (the standard HOD assumption) and still adequately fit the void statistics?

When creating density-dependent HOD models, we follow the procedure outlined in Paper I: the number density of a sample is held constant, so if  $M_{\min}$  in low-density areas increases ( $f_{\min} > 1$ ), the overall  $M_{\min}$  must decrease (slightly) to compensate for the missing low-density galaxies.

Figure 5a presents three models with  $f_{\min} = 4$  and  $\delta_c = -0.6, -0.4,$  and  $-0.2$ . Only  $\sim 8\%$  of halos with mass  $M = 10^{11.5} h^{-1} M_\odot$  reside in regions with  $\delta < -0.6$  (see Paper I, Figure 7), but the effect on the void statistics can be seen in the

lower panel of Figure 5a, which shows the residuals of the predicted VPF to the data for this model. At  $r > 5 h^{-1} \text{Mpc}$ ,  $\Delta P/\sigma_{\text{SDSS}} = 1$ , and the discrepancy monotonically increases with increasing  $r$ . For  $\delta_c = -0.4$  and  $-0.2$ , the effect can be seen clearly in the upper panel, with residuals that are larger than the scale of the lower panel. Figure 5c plots  $\chi_{\text{VPF}}^2$  as a function of  $\delta_c$  for  $f_{\min} = 2$  and 4. The gray shaded regions shows the range of  $\chi_{\text{VPF}}^2$  values from the 20 MCMC models. For  $f_{\min} = 2$ , there is no change to the VPF at  $\delta_c = -0.9$ , but as the threshold density increases,  $\chi_{\text{VPF}}^2$  rapidly increases, going from  $\chi_{\text{VPF}}^2 = 10.7$  at  $\delta_c = -0.8$  to  $\chi_{\text{VPF}}^2 = 32.5$  at  $\delta_c = -0.7$ . As noted in Paper I, the effect of increasing  $\delta_c$  ‘saturates’ at  $\delta_c \approx -0.4$ , yielding a maximum  $\chi_{\text{VPF}}^2$  of around 300. For  $f_{\min} = 4$ ,  $\chi^2$  rapidly increases at  $\delta_c \geq -0.7$  and saturates at a value of  $\sim 1200$ . The points along each  $\chi^2$  curve indicate models that produce  $b_x = 1.05$  and  $b_x = 1.1$  (from right to left). Both points lie in the saturation regime, where the discrepancies with the data are largest. In other words, in this class of  $(f_{\min}, \delta_c)$  models, one cannot alter the large scale bias factor by 5% without drastically violating constraints from the VPF. A model with  $(f_{\min}, \delta_c) = (2, -0.75)$  yields a  $\Delta\chi^2$  of 10 with respect to the standard HOD prediction.

At low  $\delta_c$ , the overall fraction of galaxies that are ‘‘moved’’ from low-density regions to median- and high-density regions is too small to affect the overall two-point clustering of the sample. As this fraction becomes non-negligible, the amplitude of the two-halo term increases as the mean bias of the sample is altered. Statistically, however, void statistics are far more sensitive to these changes in the galaxy distribution. For  $f_{\min} = 2$ ,  $\delta_c = -0.5$ , the  $\Delta\chi_{w_p}^2$  relative to the standard HOD is only 2, while  $\Delta\chi_{\text{VPF}}^2 = 210$ . Note also that the values of  $\chi_{w_p}^2$  are dependent on the value of  $\sigma_8$  assumed in the model. We have adopted a value of  $\sigma_8 = 0.9$  to match that of the simulation. A lower value of  $\sigma_8$ , consistent with new results from cosmic microwave background anisotropies (Spergel et al. 2006), could compensate for the increased amplitude of the two-halo term in  $w_p(r_p)$  for high- $\delta_c$  models. For the void statistics, no such degeneracy with  $\sigma_8$  exists; in Paper I we showed that models with  $\sigma_8 = 0.9$  and  $0.7$  yielded nearly identical void statistics, even though the lower value of  $\sigma_8$  produced a poor fit to the observed  $w_p(r_p)$ . Thus  $P_0(r)$  is both a more robust and more sensitive test to density dependence in the central galaxy occupation function.

Figures 5b and 5d compare the measured  $P_U(r)$  to the same density-dependent models in 5a and 5c. As  $\delta_c$  and  $f_{\min}$  increase, the underdense regions increase in size and frequency. The advantage of the UPF is that the effect of density dependence does not saturate at high values of  $\delta_c$ ; rather, the UPF will continue to increase as the threshold density increases. Additionally, the UPF is less susceptible to shot noise, and the percentage UPF error bars are close to half that of the VPF errors. However, this statistic is somewhat less sensitive to density dependence than the VPF because it probes moderately higher densities. While the  $f_{\min} = 2$ ,  $\delta_c = -0.5$  model yields  $\chi_{\text{VPF}}^2$  of 220, it yields  $\chi_{\text{UPF}}^2 = 25.1$ . The UPF is still more sensitive to density dependence than  $w_p(r_p)$  alone.

For brighter galaxies, the standard HOD prediction for  $P_0(r)$  for the  $M_r - 5 \log h < -21$  sample in Figures 3c and 4c yields voids that are somewhat large compared with the measured SDSS statistics. Density-dependent models with  $f_{\min} > 1$  only increase the sizes of voids and make this discrepancy more significant. Therefore, we present results for models with  $f_{\min} > 1$  and  $f_{\min} < 1$ ; in the latter models, halos in un-

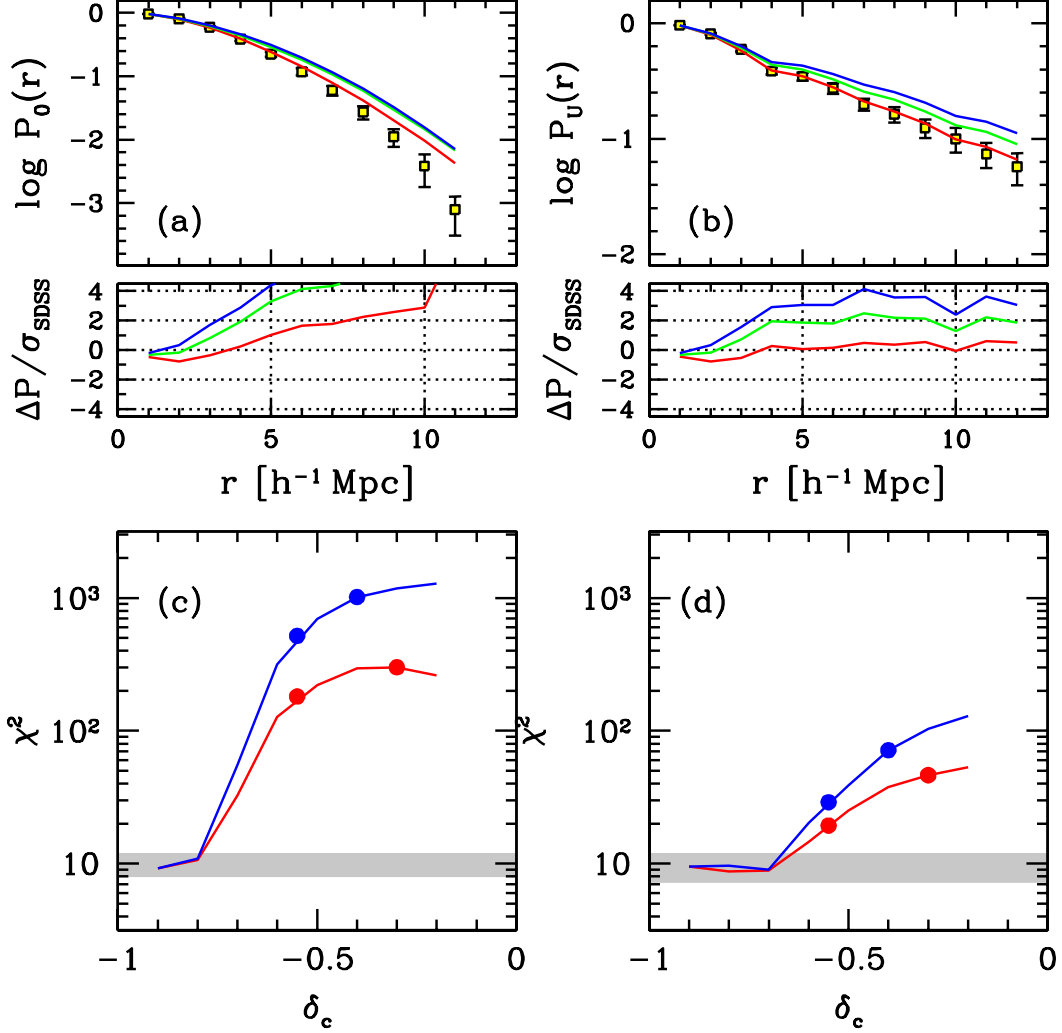


FIG. 5.— (a) Upper panel: Points with error bars are the SDSS measurements of  $P_0(r)$  for the  $M_r - 5 \log h < -19$  sample. Lines are three density-dependent HOD models with  $f_{\min} = 4$  and  $\delta_c = -0.6$  (red line),  $-0.4$  (green line), and  $-0.2$  (blue line). Bottom panel: The residuals of the model predictions relative to the data. (b) Same as (a), but for  $P_U(r)$ . (c) The  $\chi^2_{\text{VPF}}$  of the model predictions as a function of  $\delta_c$  for models with  $f_{\min} = 2$  (red line), and  $f_{\min} = 4$  (blue line). The shaded horizontal band is the range in  $\chi^2_{\text{VPF}}$  from the twenty MCMC models, all using the standard HOD implementation. Red and blue lines represent  $f_{\min} = 2$  and  $f_{\min} = 4$ , respectively. The points along each line indicate models that produce an assembly bias (in the correlation function) of 5% and 10%, from right to left. (d) Same as (c), but for the UPF.

derdense regions host (on average) more luminous galaxies at fixed halo mass. Figure 6a compares the VPFs for three different models to the SDSS data:  $(f_{\min}, \delta_c) = (2, -0.2)$ ,  $(0.5, -0.2)$  and  $(0.5, +0.2)$ . The model with  $f_{\min} = 2$  is clearly discrepant and yields residuals larger than the scale of the lower panel for  $r > 10 h^{-1} \text{Mpc}$ . The two models with  $f_{\min} = 0.5$  appear more consistent with the data than the standard HOD model in Figure 3c. The residuals are smaller at large scales, but these models tend to depress the frequency of small voids below what is measured in the SDSS. In Figure 6c, we present  $\chi^2_{\text{VPF}}$  as a function of  $\delta_c$  for models with  $f_{\min} = 0.5, 0.75, 2$  and 4. The models with  $f_{\min} > 1$  produce monotonically increasing  $\chi^2_{\text{VPF}}$  with increasing  $\delta_c$ , and are always worse fits to the data than the standard HOD. Models that produce  $b_x \geq 1.05$  yield  $\chi^2_{\text{VPF}} > 100$ . Negatively biased models with  $f_{\min} < 1$  produce a minimum at  $(f_{\min}, \delta_c) = (0.75, -0.2)$ , yielding  $\chi^2_{\text{VPF}} = 11.2$ . Figures 6b and 6d present the same results for the UPF. As with the VPF, models with  $f_{\min} < 1$  are in better agreement with  $P_U(r)$ , producing a minimum of

$\chi^2_{\text{UPF}} = 11.8$  at  $(f_{\min}, \delta_c) = (0.75, -0.2)$ , as compared with the minimum  $\chi^2_{\text{UPF}}$  of 16.5 from the MCMC models. For this model,  $b_x - 1 = -0.02$ . Models with  $b_x - 1$  of  $-0.05$ , indicated with the filled circles in Figures 6c and 6d, do not produce improved fits to the VPF of UPF.

As with the fainter samples, altering  $\langle N_{\text{cen}} \rangle_M$  in low density regions can alter the two-point clustering to some extent. The models with  $f_{\min} > 1$  produce better fits to  $w_p(r_p)$ , resulting from the increased amplitude of large-scale clustering. In the comparison of the best-fit HOD model to the SDSS  $w_p(r_p)$  data, it can be seen that the model is slightly below the measured amplitude in the two-halo regime. Thus redistributing galaxies from low to high density areas produces better agreement with the data. The models with  $f_{\min} < 1$  have the opposite effect on the two-point clustering; these models lower the bias and increase the discrepancy with the  $w_p(r_p)$  data. If we relax our constraints on the standard HOD models by setting  $\sigma_{\log M} = 0.5$ , the same result is achieved. This model yields  $\chi^2_{w_p} = 10.4$ , a value similar to that of the best density-

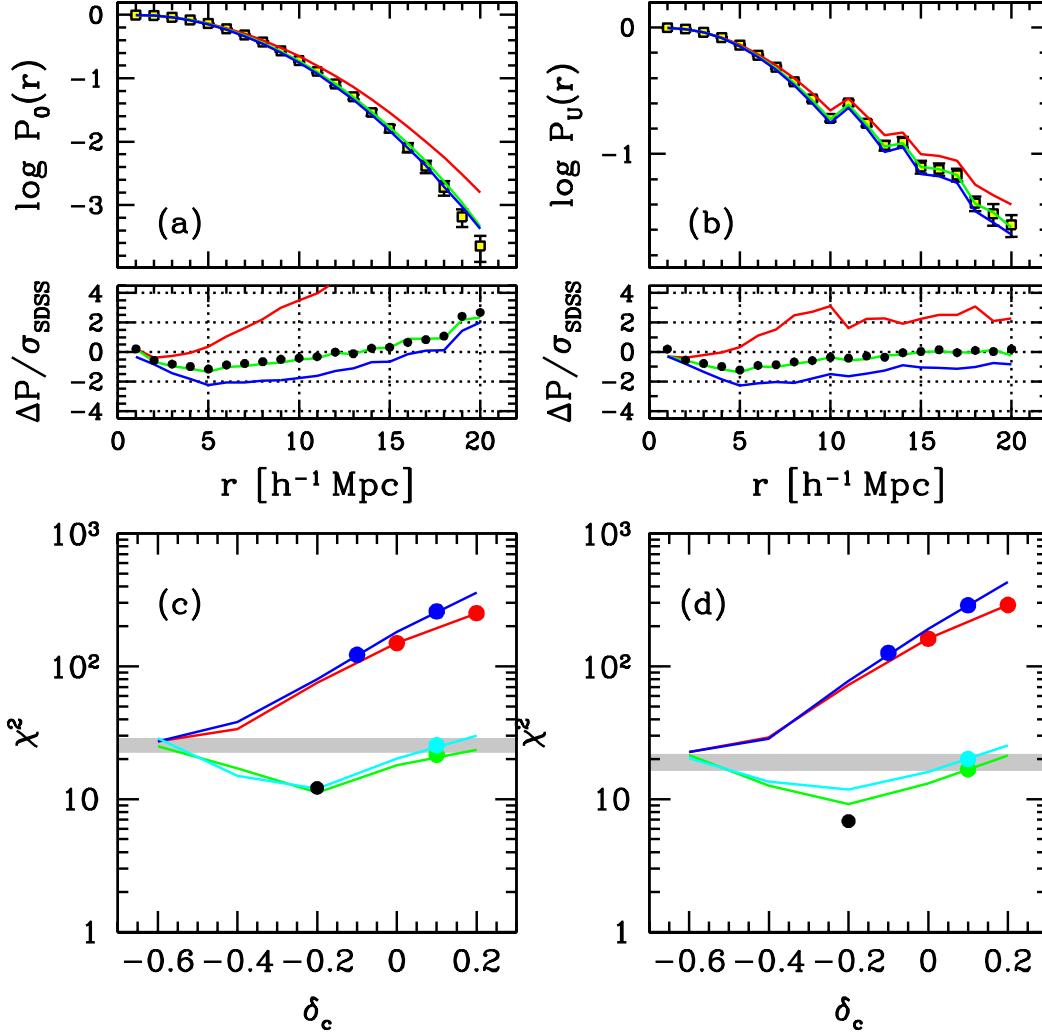


FIG. 6.— (a) Upper panel: Points with error bars represent the SDSS measurements of  $P_0(r)$  for  $M_r - 5 \log h < -21$  galaxies. Lines represent three different density-dependent HOD models,  $f_{\min} = 2$ ,  $\delta_c = -0.2$  (red line),  $f_{\min} = 0.5$ ,  $\delta_c = -0.2$  (green line), and  $f_{\min} = 0.5$ ,  $\delta_c = +0.2$  (blue line). Lower panel: The residuals of the model predictions relative to the data. The filled circles represent a standard HOD model with  $\sigma_{\log M} = 0.5$ . (b) Same as (a), but for  $P_U(r)$ . (c) The  $\chi^2_{\text{VPF}}$  of the HOD predictions for  $P_0(r)$  as a function of  $\delta_c$ . Red and blue lines represent models with  $f_{\min} = 2$  and  $f_{\min} = 4$ , respectively. Green and cyan lines represent models with  $f_{\min} = 0.75$  and  $f_{\min} = 0.5$ , respectively. The shaded horizontal line is the range in  $\chi^2_{\text{VPF}}$  from the twenty MCMC models. The filled circle represents the  $\chi^2_{\text{VPF}}$  for the model with  $\sigma_{\log M} = 0.5$  with no density dependence. Colors are the same as for the lines. Points along each line indicate models that produce and assembly bias of 5% and 10%, from right to left. For the  $f_{\min} < 1$  models, only the models with a 5% assembly bias are indicated. (d) Same as (c), but for the UPF.

dependent model ( $\chi^2_{w_p} = 11.4$ ). The high  $\chi^2_{w_p}$  is a result of the lower overall bias of the sample; the lower bias in turn produces smaller voids and yields  $P_0(r)$  and  $P_U(r)$  that are as accurate as the best density-dependent model. The residuals of the  $\sigma_{\log M} = 0.5$  are shown with the black dots in Figures 6a and 6c, and the  $\chi^2$  values for the void statistics are shown in 6d and 6d. Combining results for all data for this model,  $\chi^2_{w_p} + \chi^2_{\text{VPF}} + \chi^2_{\text{UPF}} = 29.4$  for 49 data points and 4 free parameters. This summation neglects the covariance between statistics, but it implies that a joint analysis of all data would easily find a set of HOD parameters that accurately fits both  $w_p(r_p)$  and the void statistics. Thus no strong evidence for  $f_{\min} < 1$  density dependence can be inferred.

#### 4. COLOR-DEFINED SDSS SAMPLES

##### 4.1. Results for the Standard HOD

To model the occupation function of color samples, the standard HOD parameterization presented in §2 is used to describe the overall sample, but  $\langle N_{\text{cen}} \rangle_M$  and  $\langle N_{\text{sat}} \rangle_M$  are multiplied by a coefficient that specifies the blue fraction  $f_b^{\text{cen}}$  and  $f_b^{\text{sat}}$ , respectively. The fraction of blue central galaxies is parameterized with a lognormal function of the form

$$f_b^{\text{cen}}(M) = f_0^{\text{cen}} \exp \left[ \frac{- (\log_{10} M - \log_{10} M_{\min})^2}{2(\sigma_b^{\text{cen}})^2} \right], \quad (5)$$

(cf. Z05, equation 11). Equation (5) is the same for satellite galaxies, with separate parameters for  $f_0^{\text{sat}}$  and  $\sigma_b^{\text{sat}}$ . This adds four free parameters to the HOD model, but in practice one of the new parameters is fixed by the overall blue fraction of galaxies (we choose  $f_0^{\text{cen}}$ ). We fit  $w_p(r_p)$  for the full sample, red sample, and blue sample simultaneously. These samples will be correlated, but we only use the covariance

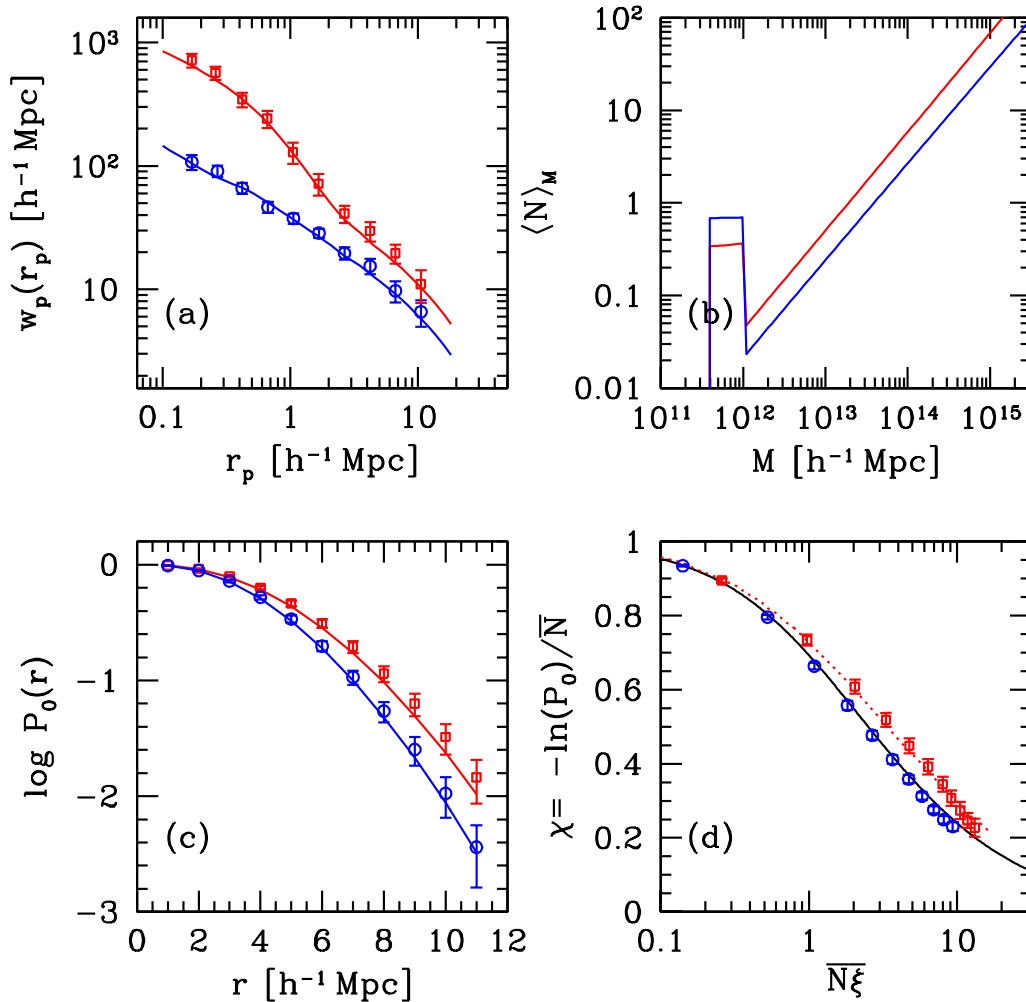


FIG. 7.— (a) Open squares with error bars show the measured  $w_p(r_p)$  for  $-20 < M_r - 5 \log h < -19$  galaxies. Red and blue points represent red galaxies and blue galaxies. The lines represent the best-fit HOD model to the data, with the same color-coordination. (b) The best-fit occupation functions for the model in panel (a). Red and blue lines plot  $\langle N \rangle_M$  for red and blue galaxies, respectively. The HOD for the full sample is the sum of these two curves. (c) Open squares with error bars show the VPFs for red and blue galaxies. Lines plot the HOD prediction for the VPF from the best-fit  $\langle N \rangle_M$  in panel (b). (d) The reduced VPF for blue and red galaxies, plotted with blue and red squares, respectively. The solid line represents the negative binomial model, which provides a good fit to the blue galaxy VPF, but the HOD prediction (dotted curve) is much more accurate for the red galaxies.

matrices of each sample independently. Using the full sample adds some complementary information to the color-only  $w_p(r_p)$  functions because it contains the cross-correlation of the red and blue galaxies.

To measure the color-dependent VPF from DR4, we adopt the same color cut as Z05,  $g - r = -0.03(M_r - 5 \log h) + 0.21$ . The fraction of blue galaxies varies significantly with luminosity. Therefore we use galaxies with magnitudes  $-19 < M_r - 5 \log h < -20$ , rather than a sample defined by a luminosity threshold, to ensure that the red and blue samples have similar mean magnitudes. We choose this sample because we wish to analyze the lowest luminosity sample for which accurate measurements can be made. Croton et al. (2007) find that the assembly bias of red galaxies monotonically increases with decreasing luminosity. The use of a magnitude bin sample necessitates an upper cutoff mass for the central occupation function, representing the mass at which halos begin hosting central galaxies too bright to be contained within the sample. For simplicity, we adopt a step function cutoff at an

upper mass limit of  $10^{12} h^{-1} M_\odot$ , obtained from fitting the  $M_r - 5 \log h < -20$  sample with a step-function  $\langle N_{\text{cen}} \rangle_M$  (i.e.,  $\sigma_{\log M} = 0$ ). Like Z05, we also set  $\sigma_{\log M} = 0$  for the magnitude bin sample, effectively making the central occupation function a square-window. Although we are fitting the same data presented in Z05 (see their Figure 23 and Table 3), we use a different linear power spectrum, and  $w_p(r_p)$  must be re-fit. We use  $\chi^2$  minimization to once again determine the best-fit model, the parameters of which are listed in Table 2.<sup>8</sup> The large values of  $\sigma_b^{\text{cen}}$  and  $\sigma_b^{\text{sat}}$  in Table 2 essentially mean that the blue galaxy fraction is a constant as a function of mass.

Figure 7a shows the results of the HOD modeling of the color-dependent clustering. The open squares plot the data from Z05 while the solid lines plot the best-fit HOD models.

<sup>8</sup> Note that the satellite occupation functions in Table 3 of Z05 assume a luminosity threshold sample. To obtain  $\langle N_{\text{sat}} \rangle_M$  for each magnitude bin,  $\langle N_{\text{sat}} \rangle_M$  for the next-brighter bin was subtracted off. The parameters of  $\langle N_{\text{sat}} \rangle_M$  in this paper are for the magnitude bin only and do not require knowledge of  $\langle N_{\text{sat}} \rangle_M$  of brighter galaxies.

Blue and red colors represent blue galaxies, red galaxies, and the full sample, respectively. The  $\chi^2_{w_p}$  for the full set of 33 data points is 11.7 (recall however that we have not taken into account the covariance between samples). The amplitude of clustering increases at all scales when comparing blue and red galaxies. The known correlation between galaxy color and environment states that red galaxies exist in more dense environments, implying that they occupy higher-mass halos that are strongly biased. Blue galaxies generally live in the field, implying that they are the central galaxies of lower-mass halos that are less strongly clustered. The best-fit occupation functions, shown in Figure 7b, bears this out. Blue galaxies dominate the central occupation function, while satellite galaxies are primarily red galaxies. These results are consistent with those in Z05.

Points in Figure 7c show the measured VPFs for red and blue galaxies. The VPF for red galaxies is significantly higher than for blue galaxies, nearly 0.5 dex at  $r = 11 h^{-1} \text{Mpc}$ . While the number density of the red sample is below that of the blue sample, diluting the blue sample randomly to match the red number density only increases the VPF at  $r = 11 h^{-1} \text{Mpc}$  by 0.04 dex; the larger voids in red galaxies are a consequence of their stronger clustering. Curves show the VPF predictions of the HOD model from Figure 7b, in which a  $\sim 10^{11.5} h^{-1} \text{M}_\odot$  halo has a  $\sim 30\%$  chance of hosting a red galaxy *independent of its large scale environment*. The agreement with the measured VPFs is strikingly good, with  $\chi^2_{\text{VPF}} = 9.89$  for red galaxies and  $\chi^2_{\text{VPF}} = 5.77$  for blue galaxies (with 10 data points in each case). We don't perform the MCMC analysis for this sample, but we expect the results to be similar to the luminosity-defined  $M_r - 5 \log h < -19$  sample in Figure 3a.

Figure 7d presents the data in the form of the reduced VPF (RVPF), in which the quantity  $\chi = -\ln(P_0)/\bar{N}$  is plotted as a function of  $\bar{N}\bar{\xi}$ , where  $\bar{N}$  is the mean number of galaxies in a sphere of radius  $r$  and  $\bar{\xi}$  is the volume-averaged two-point correlation function (in redshift space). The quantity  $\bar{\xi}$  is related to the variance of the distribution of cell counts, yielding

$$\bar{\xi} \equiv \frac{3}{r^3} \int_0^r \xi(s) s^2 ds = \frac{\langle (N - \bar{N})^2 \rangle - \bar{N}}{\bar{N}^2}. \quad (6)$$

Under the hierarchical clustering ansatz (see, e.g., Bernardeau et al. 2002), all higher-order  $n$ -point correlation functions can be written in terms of powers of the two-point correlation function and a scaling coefficient. Many different theoretical models have been proposed for the scaling coefficients (see Fry et al. 1989). Croton et al. (2004) and Conroy et al. (2005) both demonstrated that luminosity-defined samples of galaxies exhibit the void statistics predicted by a negative binomial model, in which the VPF is related to  $\bar{\xi}$  and  $\bar{N}$  by

$$P_0(r) = (1 + \bar{N}\bar{\xi})^{-1/\bar{\xi}}. \quad (7)$$

This result led Conroy et al. (2005) to conclude that the VPF contains no complementary information over the two-point correlation function for constraining galaxy bias or halo occupation.<sup>9</sup> The RVPF for blue galaxies in Figure 7d is consistent with the negative binomial model, but for red galaxies the negative binomial is not a good description of the data, in agree-

ment with the recent results from the 2dFGRS of Croton et al. (2006a). The HOD model, shown with the red dotted line, correctly predicts the behavior of the RVPF for this sample. In tests we find that occupation functions that produce correlation functions with large residuals from a power law tend to lie away from the negative binomial model in RVPF space. The high fraction of satellite galaxies in the red occupation function produces the strong transition from the one-halo to two-halo regime exhibited by red galaxies in Figure 7a, leading to the behavior seen in 7d. The correlation function for the blue sample is very close to a power law and thus is well-described by the negative binomial. This trend works in the opposite direction as well; HODs that de-emphasize high mass halos, such as those with a lower value of  $\alpha_{\text{sat}}$ , lie *below* the negative binomial curve, indicating that the negative binomial is not universal, but depends on the details of halos occupied by a given class of galaxies.

#### 4.2. Comparison to Density-Dependent Models

The assembly bias seen in the Croton et al. (2007) semi-analytical models is strongest for faint red galaxies, implying that low-mass halos that host red galaxies at their centers almost exclusively reside near a much larger halo, while in low-density environments the probability of encountering a red central galaxy is rare. To model this form of assembly bias in our HOD models, we adopt a parameterization similar to that for the luminosity-defined samples: at a density below a threshold  $\delta_c$ , the fraction of central galaxies that are red changes by a factor  $f_{\text{red}}$ .

Figure 8 shows the results for models in which  $f_{\text{red}} = 0$ , implying that there are no red galaxies below  $\delta_c$ . Figure 8a compares the  $w_p(r_p)$  data for the red sample to density-dependent models with  $\delta_c = -0.4, -0.2$ , and  $0.0$ . As with the luminosity-defined samples, the amplitude of the two-halo term in the HOD models increases as red galaxies are removed from low-density areas and redistributed in mean- and high-density environments. The model with  $\delta_c = -0.4$ , while in reasonable agreement with the  $w_p(r_p)$  data, is clearly discrepant with the VPF, yielding  $\chi^2_{\text{VPF}} = 93.2$  for 10 data points. Less extreme models,  $f_{\text{red}} = 1/8$  and  $1/4$ , still produce VPF  $\chi^2_{\text{VPF}}$  values of 60.7 and 29.4, respectively, at  $\delta_c = -0.4$ . As  $\delta_c$  increases, the discrepancy with both the VPF and  $w_p(r_p)$  data get substantially larger. Baldry et al. (2006) have investigated the environmental dependence of the halo occupation for central red galaxies in the Croton et al. (2007) model. Although their definition of environment is based on nearest-neighbor statistics, they find that the red fraction in the model decreases by nearly a factor of ten around the mean density. In Croton et al. (2007), the assembly bias for red  $M_r - 5 \log h = -19$  galaxies increases the large-scale bias of red central galaxies by a factor of 2. For the overall population of red galaxies at this magnitude, the assembly bias is  $\sim 1.25$ , comparable to the increase in  $w_p(r_p)$  in the  $f_{\text{red}} = 1/8, \delta_c = -0.2$  model, which yields  $\chi^2_{\text{VPF}} = 138$ . A more direct comparison is required to make precise statements about the form of the assembly bias in Croton et al, but the results in Figure 8 only allow for low levels of assembly bias for faint color-defined samples.

## 5. 2DFGRS RESULTS

### 5.1. 2dFGRS $w_p(r_p)$ Data and Modeling

The approach we take to apply the HOD to clustering measurements from the 2dFGRS differs slightly from that used above. 2dFGRS measurements are made on luminosity bins

<sup>9</sup> It should be noted that Conroy et al. (2005) use  $\bar{\xi}$  in redshift space; in essence they utilize more information than contained in  $w_p(r_p)$  alone. When analyzing the clustering in mock galaxy samples, those authors found that the negative binomial is not a good description of real-space clustering.

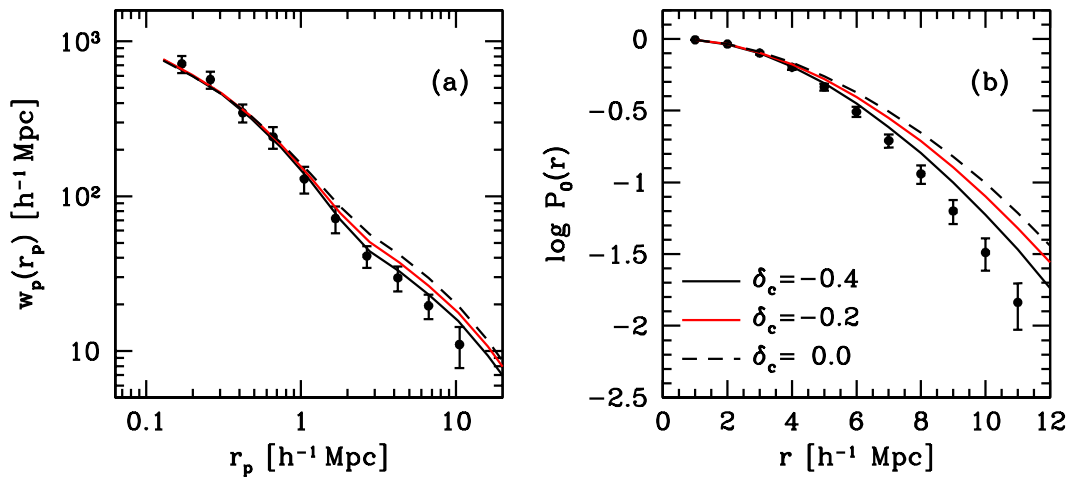


FIG. 8.— Panel (a): Data and models for  $w_p(r_p)$  for red galaxies in the  $-20 < M_r - 5 \log h < -19$  sample. Points with error bars are SDSS data. Lines are models in which the central occupation function is set to zero for halos with local densities below  $-0.4$  (black solid line),  $-0.2$  (red solid line), and  $0.0$  (dashed line). Panel (b): VPFs predicted by those same models. Points with error bars are the SDSS data from Figure 7. In both panels, the red line is a model with similar assembly bias as that found in Croton et al. (2007) for the same luminosity range.

rather than threshold samples. This necessitates a modified form of the central occupation function and a somewhat different approach to model fitting. We use the approach detailed in Tinker et al. (2007) for modeling these data. We use measurements of  $w_p(r_p)$  that have been updated from those presented in Norberg et al. (2001) and Norberg et al. (2002a) to include the full data release of the 2dFGRS (Colless et al. 2003), an increase from  $\sim 160,000$  galaxies to  $\sim 221,000$  galaxies. The details of the clustering measurements will be found in Norberg et al. (in preparation). We present here a brief summary of the calculations. Using the full 2dFGRS survey we create four volume limited samples, with faint limits from  $M_{b_j} - 5 \log h = -18.0$  to  $M_{b_j} - 5 \log h = -21.0$ , each sample 1.0 magnitudes wide. All galaxies brighter than  $M_{b_j} = -21$  are grouped into a single sample. As in Norberg et al. (2001, 2002a), a careful account of the selection function is made and the correlation functions are obtained using the standard Landy & Szalay (1993) and Hamilton (1993) estimators, with typically 100 times more randoms than galaxies. The projected correlation function is estimated by integrating  $\xi(r_p, r_\pi)$  out to  $r_{\pi, \max} = 70 h^{-1} \text{Mpc}$ , providing a stable estimate for  $w_p(r_p)$  out to at least  $r_p = 40 h^{-1} \text{Mpc}$ . Due to the sensitivity of the results on close pair incompleteness, we only use data from scales beyond  $r_p \gtrsim 150 h^{-1} \text{kpc}$ . The correlation function is measured in twelve radial bins, spaced evenly by 0.2 in  $\log_{10} r$  beginning at  $\log_{10} r = -0.7$ . The errors on the clustering measurements are estimated by a bootstrap resampling technique on roughly equal sized subregions, of which there are 16 in total (8 in each 2dFGRS region, covering in each region approximately the same survey area; see Porciani & Norberg 2006 for further details). We estimate the full covariance matrix for each sample using 100 bootstrap resamplings. The analysis in Tinker et al. (2007) was performed on bins of width 0.5 magnitudes. The bins used here are a full magnitude wide, so we redo the analysis on these new data.

In contrast to HOD models of luminosity threshold samples, binned samples require both a minimum and a maximum mass scale for central galaxies; as halo mass increases, central galaxies become brighter. The central occupation function for these samples is denoted  $\langle N_{\text{cen}} \rangle_M^i$ , where  $i$  denotes magnitude bin. The sum over all  $\langle N_{\text{cen}} \rangle_M^i$  must be less than or equal to

unity. Thus we use a modified form of equation (3) that subtracts off brighter galaxies, i.e.,

$$\begin{aligned} \langle N_{\text{cen}} \rangle_M^i &= \frac{1}{2} \left[ 1 + \text{erf} \left( \frac{\log M - \log M_{\text{min}}^i}{\sigma_{\log M}^i} \right) \right] - \langle N_{\text{cen}} \rangle_M^{i+1}, \quad 1 \leq i \leq 3, \\ \langle N_{\text{cen}} \rangle_M^i &= \frac{1}{2} \left[ 1 + \text{erf} \left( \frac{\log M - \log M_{\text{min}}^i}{\sigma_{\log M}^i} \right) \right], \quad i = 4, \end{aligned} \quad (8)$$

where  $M_{\text{min}}^i$  is the cutoff mass scale for central galaxies, and  $\sigma_{\log M}^i$  controls the width of the cutoff mass range. In equation (3),  $M_{\text{min}}$  is defined as the mass at which  $\langle N_{\text{cen}} \rangle_M = 0.5$ , but in equation (8) this mass can differ from  $M_{\text{min}}^i$ . The form we use for the satellite galaxy occupation function is

$$\langle N_{\text{sat}} \rangle_M^i = \exp \left( -\frac{M_{\text{cut}}^i}{M - M_{\text{min}}^i} \right) \left( \frac{M}{M_{\text{sat}}^i} \right)^{\alpha_{\text{sat}}} \quad (9)$$

Because information about all the bins is required to calculate  $\langle N \rangle_M^i$  for any bin  $i < 4$ , the best-fit occupation functions are determined simultaneously for all four bins. The model has 13 free parameters, with each  $M_{\text{min}}^i$  once again constrained by the number density of galaxies within each bin, calculated from the 2dFGRS luminosity function (Norberg et al. (2002b), updated to include the results from the full data release). For 48 data points, the best-fit  $\chi^2_{w_p}$  is 30.3, yielding a  $\chi^2$  per degree of freedom of 0.87. The parameters of the best-fit model are listed in Table 3. We make our predictions for the VPF by populating the  $400 h^{-1} \text{Mpc}$  box in the same manner as for the SDSS samples.

## 5.2. VPF Measurements and HOD Predictions

Measurements of the VPF for the 2dFGRS have been presented by Hoyle & Vogeley (2004), Croton et al. (2004), and Patiri et al. (2006). For the purposes of this study, none of these measurements is entirely adequate. Hoyle & Vogeley (2004) use the  $k+e$  correction of Norberg et al. (2001) in their analysis, which is significantly different than the latest  $k+e$  correction for 2dFGRS galaxies presented in Cole et al. (2005) used in the  $w_p(r_p)$  measurements described above.

TABLE 2  
BEST-FIT HOD MODEL PARAMETERS FOR SDSS GALAXIES

Sample	$\chi^2/\nu$	$M_{\min}$	$M_{\text{sat}}$	$\alpha_{\text{sat}}$	$M_{\text{cut}}$	$\sigma_{\log M}$
-19	4.89/7	$3.76 \times 10^{11}$	$9.23 \times 10^{12}$	1.11	$4.23 \times 10^9$	0.158
-20	4.77/7	$2.69 \times 10^{12}$	$2.46 \times 10^{13}$	1.13	$2.12 \times 10^{10}$	0.915
-20'	8.63/7	$9.37 \times 10^{11}$	$1.39 \times 10^{13}$	1.01	$9.54 \times 10^{12}$	0.084
-21	7.48/7	$4.89 \times 10^{12}$	$1.05 \times 10^{14}$	1.23	$3.58 \times 10^{12}$	0.052
-22	0.87/3	$1.17 \times 10^{14}$	$4.21 \times 10^{14}$	1.20	$2.40 \times 10^{14}$	0.615
[-19,-20]	11.7/28	$3.91 \times 10^{11}$	$1.32 \times 10^{13}$	1.06	—	—
[-19,-20]		$\sigma_b^{\text{cen}}$ 7.97	$f_b^{\text{cen}}$ 0.68	$\sigma_b^{\text{sat}}$ 9.46	$f_b^{\text{sat}}$ 0.33	

NOTE. — All masses are in units of  $h^{-1} M_{\odot}$ . The bottom two rows are parameters for modeling color-selected samples. See §4 for a discussion.

TABLE 3  
BEST-FIT HOD MODEL PARAMETERS FOR 2DFGRS GALAXIES

Sample	$\chi^2$	$M_{\min}^i$	$M_{\text{sat}}^i$	$M_{\text{cut}}^i$	$\sigma_{\log M}^i$
[-18.0, -19.0]	5.7	$2.79 \times 10^{11}$	$9.19 \times 10^{12}$	$5.07 \times 10^{11}$	0.25
[-19.0, -20.0]	10.0	$6.14 \times 10^{11}$	$1.50 \times 10^{13}$	$1.55 \times 10^{12}$	0.07
[-20.0, -21.0]	8.8	$3.15 \times 10^{12}$	$4.23 \times 10^{13}$	$1.35 \times 10^{13}$	0.23
< -21.0	5.8	$5.21 \times 10^{13}$	$3.55 \times 10^{14}$	$1.27 \times 10^{14}$	0.53

NOTE. — All masses are in units of  $h^{-1} M_{\odot}$ . All samples are analyzed simultaneously, so  $\chi^2/\nu = 30.3/(48 - 13) = 0.87$ .

This leads to a difference in the number densities of galaxies between the  $w_p(r_p)$  samples and the  $P_0(r)$  samples. This difference becomes larger with the mean redshift of the sample, and the  $M_{b_j} - 5 \log h < -21$  sample in Hoyle & Vogeley (2004) has more than twice as many galaxies in it as the sample analyzed here. Note that the effect of this mismatch is quite different from the difference in number densities in the SDSS samples and the HOD models in §3. That discrepancy is due to the survey selection function, but Hoyle & Vogeley (2004) essentially analyze different sets of galaxies, which have different clustering and void statistics. Thus one would not expect our HOD predictions to match their  $P_0(r)$  measurements, even if we adjusted our models to match their  $\bar{n}_g$ . For the Croton et al. (2004) data, the completeness correction applied to them accrues an unquantified systematic error that is difficult to model. Their measurements also employ an outdated  $k+e$  correction from Norberg et al. (2002b), although the differences between this correction and the Cole et al. (2005) correction are substantially smaller. Patiri et al. (2006) construct volume-limited samples within the 2dFGRS with magnitude thresholds of  $M_{b_j} - 5 \log h < -19.32$  and  $M_{b_j} - 5 \log h < -20.181$ , values that do not correspond to the unit magnitude bins of our  $w_p(r_p)$  measurements. Thus for comparison with our HOD predictions we repeat the analysis of Patiri et al. (2006), making several adjustments to better facilitate the comparison. We use the Cole et al. (2005)  $k+e$  correction, and all galaxies are corrected to  $z=0.1$ . We construct volume-limited samples that match our  $w_p(r_p)$  samples, and we keep track of the number density of galaxies at each  $r$  in order to repeat the procedure used above for comparing to SDSS data.

We create HOD predictions by populating the  $400 h^{-1}$  Mpc simulation with the best-fit HOD parameters for each magnitude bin and scaling the number density at each  $r$  to the value measured, as with the SDSS data. Error bars on the data are also obtained from this simulation. The mean incompleteness

of the 2dFGRS is larger than in the SDSS, and the variation of  $\bar{n}_g(r)$  is also larger. We are unable to use the  $1086 h^{-1}$  Mpc box for modeling the brighter two samples because the occupation functions extend below the resolution limit of that simulation. For these reasons, we do not perform a detailed statistical analysis as with the SDSS samples, but rather compare the data and models more qualitatively.

Figure 9a and 9b show the results for the  $-19 < M_{b_j} - 5 \log h < -18$  and  $-20 < M_{b_j} - 5 \log h < -19$  magnitude bins. The best-fit HOD model accurately predicts the the VPF for these two samples. Figure 9c shows the results for  $-21 < M_{b_j} - 5 \log h < -20$ . The model slightly over-predicts  $P_0(r)$  for  $r \geq 10 h^{-1}$  Mpc in much the same way as the  $M_r - 5 \log h < -21$  SDSS sample but with smaller significance (with respect to diagonal error bars only). For the brightest 2dFGRS galaxies in Figure 9d, our model is a poor fit to the observed VPF. The voids in the data are clearly much smaller than those predicted by the HOD. As a rough guide, the diagonal-only  $\chi_{\text{diag}}^2 = 338$  for the best-fit  $w_p(r_p)$  model (not shown in this Figure). These rare galaxies reside in rare, highly biased halos and the model predictions are more sensitive to the value of  $\sigma_{\log M}$  than for other samples. To explore this effect, we analyze this sample separately in an MCMC chain. The upper and lower bounds of the shaded region are models from the chain with the lowest and highest values, respectively, of  $\sigma_{\log M}$  with  $\Delta\chi_{w_p}^2 < 1$  with respect to the best-fit model. The lower bound, with  $\sigma_{\log M} = 0.9$ , lies closer to the data but is still significantly discrepant. Although it is possible to construct density dependent models to match the measured  $P_0(r)$ , these models will be highly discrepant with the measurements of  $w_p(r_p)$  since they require an increase in the galaxy formation efficiency in lower density regions. Berlind et al. (2006) investigated the clustering of massive galaxy groups, demonstrating that at fixed mass, systems with bluer central galaxies are more strongly clustered than redder central galaxies. Be-

cause 2dFGRS is a blue-selected survey, the effect of density dependence would make the voids in the brightest 2dFGRS galaxies larger than in the standard HOD, the opposite of the discrepancy in Figure 9d.

The conflict in 9d can be resolved if the brightest 2dFGRS galaxies are not always in the most massive halos. The solid line in Figure 9d represents a model for this sample in which the maximum value of  $\langle N_{\text{cen}} \rangle_M$  for this model is 0.5 rather than unity. Equation (8) is modified by a simple multiplicative factor of 0.5, preserving the shape of the cutoff. Physically this model implies that the relationship between host halo mass and central galaxy luminosity  $L_c$  becomes essentially flat at  $M \gtrsim 10^{14} h^{-1} M_\odot$  in  $b_J$ . Setting the maximum value of  $\langle N_{\text{cen}} \rangle_M$  to 0.5 reduces  $M_{\text{min}}$  for this sample in order to match the number density and the overall bias of the model is reduced. This model is conceptually similar to one with a very large value of  $\sigma_{\log M}$ , large enough such that  $\langle N_{\text{cen}} \rangle_M$  never reaches unity at the largest resolved halos. But due to the functional form of equation (8) values of  $\sigma_{\log M}$  large enough to resolve the discrepancy with the  $P_0(r)$  data place a non-negligible fraction of the brightest galaxies in  $\sim 10^8 h^{-1} M_\odot$  halos, which is both physically unreasonable and significantly lowers the amplitude of  $w_p(r_p)$ . The large-scale amplitude of the low- $\langle N_{\text{cen}} \rangle_M$  model is also below that of the fiducial model, but the increase in  $\chi_{w_p}^2$  is a modest  $\sim 2$ . The effect on the void statistics is marked: the low- $\langle N_{\text{cen}} \rangle_M$  model VPF is in good agreement with the observations. The lower-bound of the shaded region in Figure 9d (the model with  $\sigma_{\log M} = 0.9$ ) yields  $\chi_{\text{diag}}^2 = 91.3$ , while the low- $\langle N_{\text{cen}} \rangle_M$  model yields  $\chi_{\text{diag}}^2 = 35.3$ . To properly compare these models, larger simulations with the proper mass resolution are required to estimate the covariance matrices, but it is clear that the low- $\langle N_{\text{cen}} \rangle_M$  model is an improvement. The clustering of the galaxies in the next-brightest bin are unaffected by this change in the HOD; although fainter galaxies can occupy the highest mass halos, the overall number of these galaxies is insignificant, and both  $w_p(r_p)$  and  $P_0(r)$  are unchanged.

For galaxy groups in the 2dFGRS, Yang et al. (2005) find that  $L_c$  increases with halo mass as  $M^{2/3}$  at low masses, but becomes shallower for  $M > 10^{13} h^{-1} M_\odot$ , increasing as  $M^{1/4}$ . At  $M > 10^{14} h^{-1} M_\odot$ , the mass at which  $\langle N_{\text{cen}} \rangle_M$  reaches its maximum, the scatter in the  $L_c - M$  relation becomes large, covering nearly half a dex in  $L_c$ . For redder bands like Sloan- $r$ , a continual monotonic relation between  $L_c$  and  $M$  is well motivated, but just due to the width of the color-magnitude relation some galaxies from a lower  $M_r$  magnitude bin will fall in the brightest  $b_J$  bin. As Cole et al. (2006) recently pointed out, the color distributions of the SDSS and 2dFGRS are substantially different, with the SDSS being dominated by red galaxies and the 2dFGRS dominated by blue objects. Convolved with the magnitude errors of the 2dFGRS, which are larger than those in the SDSS (and will scatter asymmetrically from lower luminosities to higher luminosities), a complete sample of the brightest  $M_r$  galaxies in one survey may not contain all of the brightest  $b_J$  galaxies in the other.

## 6. DISCUSSION

In this paper we have demonstrated that an environmentally independent approach to halo occupation can simultaneously model both the two-point clustering and the void statistics of galaxy samples selected by both luminosity and color. Because  $w_p(r_p)$  and  $P_0(r)$  weight environments differently, with  $w_p(r_p)$  determined predominantly by halos that sit at or above

the mean density and  $P_0(r)$  determined by halos that reside in low-density regions, our results show that, to the limit these statistics can be measured,  $\langle N_{\text{cen}} \rangle_M$  is independent of environment. Although we are not explicitly testing environmental dependence of satellite galaxy occupation, the results in the paper offer an implicit test: If the number of satellite galaxies strongly correlates with halo environment, then the HOD inferred from modeling  $w_p(r_p)$  will be systematically biased and could predict the wrong void distribution regardless of whether central galaxies exhibit assembly bias. In Paper I we demonstrated that  $w_p(r_p)$  constrains the fraction of galaxies that are satellites, and thus the complementary fraction that are central. The central galaxy fraction, in turn, strongly influences the distribution of void sizes. If the HOD model for  $w_p(r_p)$  is systematically under- or overestimating this quantity, then the predicted void statistics will not match observations.

It has been suggested that voids and void galaxies represent a challenge to the  $\Lambda$ CDM model (Peebles 2001). If there exists substantial mass in underdense regions, the argument goes, then the observed paucity of low-luminosity galaxies in these regions is incompatible with the standard hierarchical clustering picture because low-mass halos in the voids will contain low-luminosity galaxies. Wechsler et al. (2006) propose that the assembly bias of low mass halos may be related to this so-called ‘void phenomenon’, because low mass halos in underdense regions form later, and the gas within them may therefore form stars less efficiently due to an increased photoionizing background. Our results suggest that there is no void phenomenon for galaxies as faint as  $\sim 0.2L_*$  (a halo mass of  $\sim 0.02M_*$ , the minimum mass probed in the Wechsler et al. 2006 results). The observed voids in samples of low-luminosity galaxies match the voids predicted by the typical halos those galaxies occupy. The data presented here leave little room for a shift in galaxy formation efficiency (or a shift in the typical halo occupied) in low-density regions. These results are in agreement with the results of semi-analytic models of Mathis & White (2002) and Benson et al. (2003), which find that low luminosity galaxies avoid the voids defined by the brighter galaxies. As Wechsler et al. (2006) suggest, assembly bias may influence the formation of fainter void galaxies, but larger observational samples are required to fully address this problem.

In the semi-analytic results of Croton et al. (2007), the impact of the assembly bias on the correlation function ranges from  $b_x - 1 = 0.05$  for faint galaxies to  $b_x - 1 = -0.05$  for bright samples. We have shown that, at least in the class of  $(f_{\text{min}}, \delta_c)$  models considered here, assembly bias of this order for central galaxies cannot be reconciled with the measured void statistics. Density dependent models that produce acceptable fits to  $P_0(r)$  and  $P_U(r)$  produce values of  $|b_x - 1| \leq 0.02$ . At some level, assembly bias should be present in the galaxy population, but we have ruled out a strong dependence of  $\langle N_{\text{cen}} \rangle_M$  on  $\delta$  that could bias measurements of halo occupation parameters or constraints on cosmological parameters obtained through the application of the HOD. At the level of precision of the current generation of large-scale redshift surveys, our results suggest that assembly bias is generally not a concern, though it could still have some influence on statistical measures not constrained (directly or indirectly) by our analysis. The assembly bias issue will need to be revisited for accurate analysis of the next generation of galaxy redshift surveys, when percent-level effects become significant.

For luminosity samples, it is perhaps not unexpected that

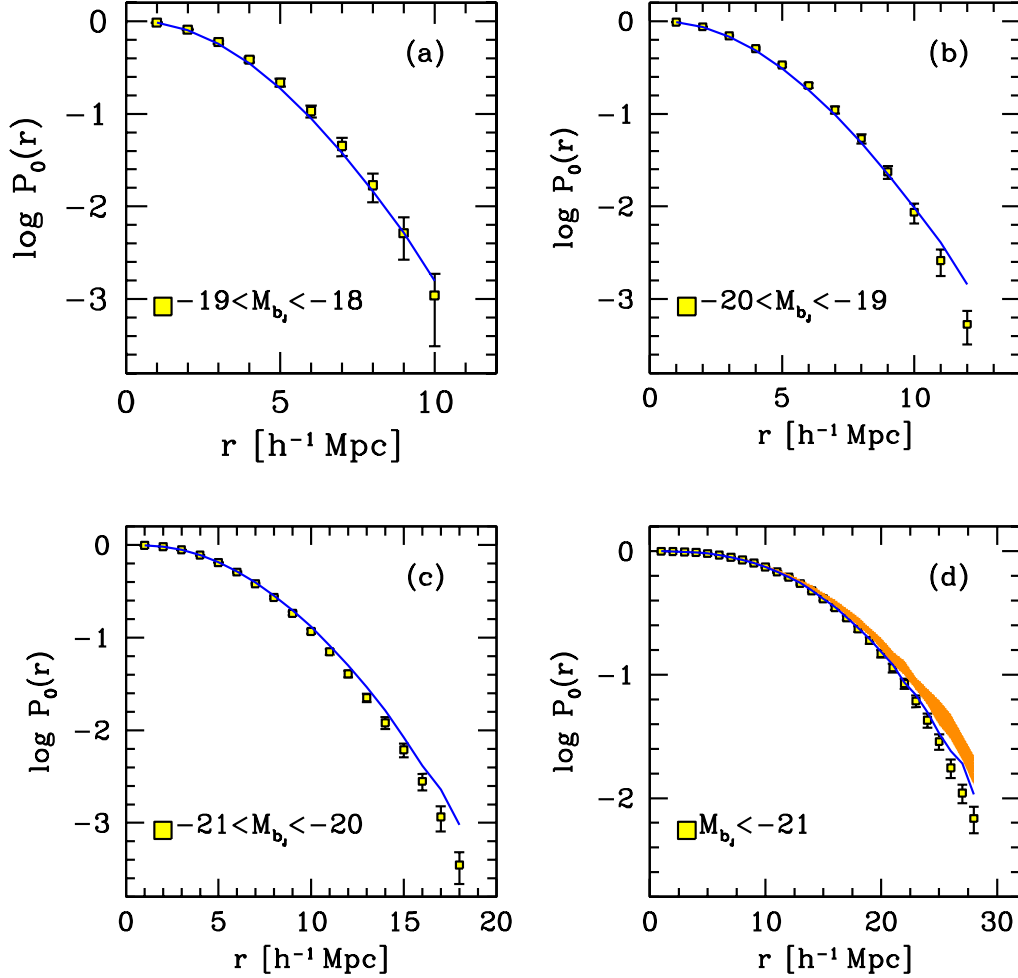


FIG. 9.— Panels (a)–(c) show a comparison between 2dFGRS VPF data and HOD model predictions. Points with error bars observational measurements. Solid lines are the HOD predictions from the best-fit model, obtained from the  $400 h^{-1}$  Mpc box. In panel (d), the points show the 2dFGRS data, while the shaded region shows the range of predictions for models with the highest and lowest values of  $\sigma_{\log M}$  that produce a  $\Delta\chi_{w,p}^2 < 1$  with respect to the best-fit model, which has a value of  $\sigma_{\log M} = 0.53$ . The lower bound represents a model with  $\sigma_{\log M} = 0.9$ , and the upper bound represents a model with  $\sigma_{\log M} = 0.05$ . The solid line is a model in which the maximum value of  $\langle N_{\text{cen}} \rangle_M$  is 0.5, as opposed to 1 for the other models. This low- $\langle N_{\text{cen}} \rangle_M$  model has a value of  $\sigma_{\log M} = 0.73$ .

environmental effects are small. For color-defined samples, on the other hand, our results are more surprising. Because halo formation time depends so strongly on local density, with younger low mass halos living in low density regions, one might naturally expect the stellar populations within these halos to reflect this trend. This would lead to an assembly bias such that, at fixed mass, the lower the local density, the larger the fraction of central galaxies that are blue in color. This is exactly the type of bias seen in the models of Croton et al. (2007): low mass halos with red central galaxies form near  $z \sim 2$ , while low mass halos with blue central galaxies have formation redshifts of  $z \sim 1.5$  or less. However, in our “standard” HOD analysis of color-defined samples, we assume that the red central galaxy fraction is independent of environment. Equation (5) implies, when applied to the samples explored §4, that a  $\sim 10^{11.5} h^{-1} M_{\odot}$  halo has a  $\sim 30\%$  chance of hosting a red central galaxy regardless of environment or formation time. In Croton et al. (2007), assembly bias results in voids in the red galaxies that are significantly larger than in

the HOD prediction. The results of Figures 7 and 8 support a central red fraction that is environment independent. In contrast to luminosity-defined samples, the current precision of the SDSS is sufficient to exclude the level of assembly bias measured in Croton et al. (2007) for color-defined samples, which in their model is driven primarily by central galaxies.

Inconsistencies between observed properties of the red galaxy population and the predictions of Croton et al. (2007) have been reported elsewhere as well. Springel et al. (2005) show that the amplitude of the two-point correlation function of red galaxies in the Millennium Run semi-analytic galaxy population is much higher than observations at all scales. Weinmann et al. (2006), using a catalog of galaxy groups created from the SDSS, demonstrate that the red galaxy fraction of groups is too high in the Croton et al. (2006b) model. Baldry et al. (2006) investigate the red fraction as a function of local galaxy density in the SDSS, measuring a monotonic decrease in red fraction with decreasing density. Such a correlation can naturally result from the dependence of the halo

mass function of local environment without invoking assembly bias (Berlind et al. 2005): red galaxies are primarily satellites in high mass halos (see Figure 7b), and the frequency of such halos correlates strongly with local density. Baldry et al. (2006) find that the correlation of red galaxy fraction with environment is much steeper in the Croton et al. (2006b) model than measured in the SDSS. They show that this result is primarily due to the correlation between red central galaxies and environment. Although Baldry et al. define density by local galaxy density in redshift space using a nearest neighbor criterion, the relation they find in the Croton et al. (2006b) model between the red fraction of central galaxies and density is similar to the models tested in §3.3 with a sharp decrease in red central fraction by nearly an order of magnitude at densities below the mean.

These discrepancies between semi-analytic models and observations offer insight into galaxy formation processes. The aspect of the Croton et al. (2006b) model that most directly influences galaxy color is its treatment of AGN feeding and feedback, which heats the gas and halts star formation. In the model, this mechanism is correlated with environment to produce the color-dependent assembly bias. This work, and the papers listed above, suggest that a gas-heating mechanism less sensitive to halo environment will bring the models into better agreement with the clustering data.

Regardless of the details of galaxy formation, it is well-established now that correlations exist between halo properties and environment, especially for the low-mass halos that contain  $M_r - 5 \log h \sim -19$  galaxies. Gao & White (2006) show that environment correlates with halo formation time, concentration, and spin for  $M < M_*$ . Why then is the correlation with galaxy properties so weak? To produce the observed void statistics, the luminosity of a central galaxy must be largely uncorrelated with halo properties other than mass, in the sense that the correlation must be significantly smaller than the scatter in  $L_c$  at a given halo formation time or formation history. Additionally, central galaxy color must also be weakly correlated with halo formation. The amount of star formation required to make a red galaxy blue is relatively small, while the amount of time required for a blue galaxy

to passively evolve into a red object can be  $\lesssim 1$  Gyr (see Faber et al. 2005 and references therein). If the color distribution is determined mainly by the occurrence of recent star formation, galaxy colors may be a stochastic process in better agreement with the assumptions of the HOD. Rojas et al. (2004, 2005) find that void galaxies have higher specific star formation rates than galaxies in higher-density environments. As with the color-density relation (Berlind et al. (2005)), the correlation of star formation rate with environment may reflect changes in the underlying halo mass function between low and high densities rather than a correlation with formation history.

The nature of voids has been an important question since their discovery in the first large galaxy redshift survey (Gregory & Thompson 1978; Kirshner et al. 1981). Are voids truly empty of matter or just deficient in galaxies? Is a non-gravitational process required to explain their observed sizes? These questions have become better defined through convergence on a standard cosmological model and better understanding of the relation between galaxies and dark matter halos. We find that the sizes and emptiness of observed voids are in excellent agreement with straightforward theoretical predictions.

The authors wish to thank Darren Croton, Brant Robertson, Ravi Sheth, Michael Vogeley, Risa Wechsler, Martin White, and Andrew Zentner for many useful discussions. JLT acknowledges the use of the computing facilities of the Department of Astronomy at Ohio State University. JLT also would like to acknowledge the generous hospitality of the Institute for Computational Cosmology at the University of Durham, where part of this work was completed. DW acknowledges the support of NSF grant AST-0407125. Portions of this work were performed under the auspices of the U.S. Dept. of Energy, and supported by its contract #W-7405-ENG-36 to Los Alamos National Laboratory. Computational resources were provided by the LANL open supercomputing initiative. CC thanks the Instituto de Astrofísica de Andalucía (CSIC) for their wonderful espresso bar and financial support in the Spring of 2006.

#### REFERENCES

- Abazajian, K., Zheng, Z., Zehavi, I., Weinberg, D. H., Frieman, J. A., Berlind, A. A., Blanton, M. R., Bahcall, N. A., Brinkmann, J., Schneider, D. P., & Tegmark, M. 2005, *ApJ*, 625, 613
- Abazajian, K. et al. 2004, *AJ*, 128, 502
- Abbas, U. & Sheth, R. K. 2005, *MNRAS*, 364, 1327
- . 2006, *MNRAS*, accepted, (astro-ph/0601407)
- Adelman-McCarthy, J. K. et al. 2006, *ApJS*, 162, 38
- Baldry, I. K., Balogh, M. L., Bower, R. G., Glazebrook, K., Nichol, R. C., Bamford, S. P., & Budavari, T. 2006, *MNRAS*, 373, 469
- Baugh, C. M., Croton, D. J., Gaztañaga, E., Norberg, P., Colless, M., Baldry, I. K., Bland-Hawthorn, J., Bridges, T., Cannon, R., Cole, S., Collins, C., Couch, W., Dalton, G., De Propris, R., Driver, S. P., Efstathiou, G., Ellis, R. S., Frenk, C. S., Glazebrook, K., Jackson, C., Lahav, O., Lewis, I., Lumsden, S., Maddox, S., Madgwick, D., Peacock, J. A., Peterson, B. A., Sutherland, W., & Taylor, K. 2004, *MNRAS*, 351, L44
- Benson, A. J. 2001, *MNRAS*, 325, 1039
- Benson, A. J., Cole, S., Frenk, C. S., Baugh, C. M., & Lacey, C. G. 2000, *MNRAS*, 311, 793
- Benson, A. J., Hoyle, F., Torres, F., & Vogeley, M. S. 2003, *MNRAS*, 340, 160
- Berlind, A. A., Blanton, M. R., Hogg, D. W., Weinberg, D. H., Davé, R., Eisenstein, D. J., & Katz, N. 2005, *ApJ*, 629, 625
- Berlind, A. A., Kazin, E., Blanton, M. R., Pueblas, S., Scoccimarro, R., & Hogg, D. W. 2006, *The Clustering of Galaxy Groups: Dependence on Mass and Other Properties*
- Berlind, A. A. & Weinberg, D. H. 2002, *ApJ*, 575, 587
- Bernardeau, F., Colombi, S., Gaztañaga, E., & Scoccimarro, R. 2002, *Phys. Rep.*, 367, 1
- Blanton, M. R., Berlind, A. A., & Hogg, D. W. 2006a, *ApJ*, submitted, (astro-ph/0608353)
- Blanton, M. R., Eisenstein, D., Hogg, D. W., Schlegel, D. J., & Brinkmann, J. 2005a, *ApJ*, 629, 143
- Blanton, M. R., Eisenstein, D., Hogg, D. W., & Zehavi, I. 2006b, *ApJ*, 645, 977
- Blanton, M. R., Hogg, D. W., Bahcall, N. A., Brinkmann, J., Britton, M., Connolly, A. J., Csabai, I., Fukugita, M., Loveday, J., Meiksin, A., Munn, J. A., Nichol, R. C., Okamura, S., Quinn, T., Schneider, D. P., Shimasaku, K., Strauss, M. A., Tegmark, M., Vogeley, M. S., & Weinberg, D. H. 2003, *ApJ*, 592, 819
- Blanton, M. R. & Rowies, S. 2006, *ApJ*, submitted, (astro-ph/0606170)
- Blanton, M. R., Schlegel, D. J., Strauss, M. A., Brinkmann, J., Finkbeiner, D., Fukugita, M., Gunn, J. E., Hogg, D. W., Ivezić, Ž., Knapp, G. R., Lupton, R. H., Munn, J. A., Schneider, D. P., Tegmark, M., & Zehavi, I. 2005b, *AJ*, 129, 2562
- Bullock, J. S., Kolatt, T. S., Sigad, Y., Somerville, R. S., Kravtsov, A. V., Klypin, A. A., Primack, J. R., & Dekel, A. 2001, *MNRAS*, 321, 559
- Cole, S., Percival, W. J., Peacock, J. A., Norberg, P., Baugh, C. M., Frenk, C. S., Baldry, I., Bland-Hawthorn, J., Bridges, T., Cannon, R., Colless, M., Collins, C., Couch, W., Cross, N. J. G., Dalton, G., Eke, V. R., De Propris, R., Driver, S. P., Efstathiou, G., Ellis, R. S., Glazebrook, K., Jackson, C., Jenkins, A., Lahav, O., Lewis, I., Lumsden, S., Maddox, S., Madgwick, D., Peterson, B. A., Sutherland, W., & Taylor, K. 2005, *MNRAS*, 362, 505
- Cole, S., Sanchez, A. G., & Wilkins, S. 2006, *ASP conference series: Cosmic Frontiers*, in press (astro-ph/0611178)
- Colless, M., Dalton, G., Maddox, S., Sutherland, W., Norberg, P., Cole, S., Bland-Hawthorn, J., Bridges, T., Cannon, R., Collins, C., Couch, W., Cross, N., Deeley, K., De Propris, R., Driver, S. P., Efstathiou, G., Ellis, R. S., Frenk, C. S., Glazebrook, K., Jackson, C., Lahav, O., Lewis, I., Lumsden, S., Madgwick, D., Peacock, J. A., Peterson, B. A., Price, I., Seaborn, M., & Taylor, K. 2001, *MNRAS*, 328, 1039

- Colless, M., Dalton, G., Maddox, S., Sutherland, W., Norberg, P., Cole, S., Bland-Hawthorn, J., Bridges, T., Cannon, R., Collins, C., Couch, W., Cross, N., Deeley, K., de Propriis, R., Driver, S. P., Efstathiou, G., Ellis, R. S., Frenk, C. S., Glazebrook, K., Jackson, C., Lahav, O., Lewis, I., Lumsden, S., Madgwick, D., Peacock, J. A., Peterson, B. A., Price, I., Seaborne, M., & Taylor, K. 2003, *VizieR Online Data Catalog*, 7226, 0
- Conroy, C., Coil, A. L., White, M., Newman, J. A., Yan, R., Cooper, M. C., Gerke, B. F., Davis, M., & Koo, D. C. 2005, *ApJ*, 635, 990
- Croton, D. J., Colless, M., Gaztañaga, E., Baugh, C. M., Norberg, P., Baldry, I. K., Bland-Hawthorn, J., Bridges, T., Cannon, R., Cole, S., Collins, C., Couch, W., Dalton, G., de Propriis, R., Driver, S. P., Efstathiou, G., Ellis, R. S., Frenk, C. S., Glazebrook, K., Jackson, C., Lahav, O., Lewis, I., Lumsden, S., Maddox, S., Madgwick, D., Peacock, J. A., Peterson, B. A., Sutherland, W., & Taylor, K. 2004, *MNRAS*, 352, 828
- Croton, D. J., Gao, L., & White, S. D. M. 2007, *MNRAS*, 374, 1303
- Croton, D. J., Norberg, P., Gaztanaga, E., & Baugh, C. M. 2006a, *MNRAS*, submitted (astro-ph/0611313)
- Croton, D. J., Springel, V., White, S. D. M., De Lucia, G., Frenk, C. S., Gao, L., Jenkins, A., Kauffmann, G., Navarro, J. F., & Yoshida, N. 2006b, *MNRAS*, 365, 11
- Davis, M., Efstathiou, G., Frenk, C. S., & White, S. D. M. 1985, *ApJ*, 292, 371
- Dressler, A. 1980, *ApJ*, 236, 351
- Faber, S. M., Willmer, C. N. A., Wolf, C., Koo, D. C., Weiner, B. J., Newman, J. A., Im, M., Coil, A. L., Conroy, C., Cooper, M. C., Davis, M., Finkbeiner, D. P., Gerke, B. F., Gebhardt, K., Groth, E. J., Guhathakurta, P., Harker, J., Kaiser, N., Kassin, S., Kleinheinrich, M., Konidaris, N. P., Lin, L., Luppino, G., Madgwick, D. S., Noeske, K. M. K. G., Phillips, A. C., Sarajedini, V. L., Simard, L., Szalay, A. S., Vogt, N. P., & Yan, R. 2005, *Galaxy Luminosity Functions to z1: DEEP2 vs. COMBO-17 and Implications for Red Galaxy Formation*
- Fry, J. N., Giovanelli, R., Haynes, M. P., Melott, A. L., & Scherrer, R. J. 1989, *ApJ*, 340, 11
- Gao, L., Springel, V., & White, S. D. M. 2005, *MNRAS*, 363, L66
- Gao, L. & White, S. D. M. 2006
- Gaztañaga, E., Norberg, P., Baugh, C. M., & Croton, D. J. 2005, *MNRAS*, 364, 620
- Gott, J. R. I., Jurić, M., Schlegel, D., Hoyle, F., Vogeley, M., Tegmark, M., Bahcall, N., & Brinkmann, J. 2005, *ApJ*, 624, 463
- Gregory, S. A. & Thompson, L. A. 1978, *ApJ*, 222, 784
- Hamilton, A. J. S. 1993, *ApJ*, 417, 19
- Hamilton, A. J. S. & Tegmark, M. 2004, *MNRAS*, 349, 115
- Harker, G., Cole, S., Helly, J., Frenk, C. S., & Jenkins, A. 2005, *MNRAS*, Submitted (astro-ph/0510488)
- Hoyle, F. & Vogeley, M. S. 2004, *ApJ*, 607, 751
- Jenkins, A., Frenk, C. S., White, S. D. M., Colberg, J. M., Cole, S., Evrard, A. E., Couchman, H. M. P., & Yoshida, N. 2001, *MNRAS*, 321, 372
- Jing, Y. P., Mo, H. J., & Boerner, G. 1998, *ApJ*, 494, 1
- Kauffmann, G., Nusser, A., & Steinmetz, M. 1997, *MNRAS*, 286, 795
- Kirshner, R. P., Oemler, Jr., A., Schechter, P. L., & Shectman, S. A. 1981, *ApJ*, 248, L57
- Landy, S. D. & Szalay, A. S. 1993, *ApJ*, 412, 64
- Lemson, G. & Kauffmann, G. 1999, *MNRAS*, 302, 111
- Little, B. & Weinberg, D. H. 1994, *MNRAS*, 267, 605
- Ma, C.-P. & Fry, J. N. 2000, *ApJ*, 543, 503
- Mathis, H. & White, S. D. M. 2002, *MNRAS*, 337, 1193
- Navarro, J., Frenk, C., & White, S. 1997, *ApJ*, 490, 493
- Nichol, R. C., Sheth, R. K., Suto, Y., Gray, A. J., Kayo, I., Wechsler, R. H., Marin, F., Kulkarni, G., Blanton, M., Connolly, A. J., Gardner, J. P., Jain, B., Miller, C. J., Moore, A. W., Pope, A., Pun, J., Schneider, D., Schneider, J., Szalay, A., Szapudi, I., Zehavi, I., Bahcall, N. A., Csabai, I., & Brinkmann, J. 2006, *MNRAS*, submitted, (astro-ph/0602548)
- Norberg, P., Baugh, C. M., Hawkins, E., Maddox, S., Madgwick, D., Lahav, O., Cole, S., Frenk, C. S., Baldry, I., Bland-Hawthorn, J., Bridges, T., Cannon, R., Colless, M., Collins, C., Couch, W., Dalton, G., De Propriis, R., Driver, S. P., Efstathiou, G., Ellis, R. S., Glazebrook, K., Jackson, C., Lewis, I., Lumsden, S., Peacock, J. A., Peterson, B. A., Sutherland, W., & Taylor, K. 2002a, *MNRAS*, 332, 827
- Norberg, P., Baugh, C. M., Hawkins, E., Maddox, S., Peacock, J. A., Cole, S., Frenk, C. S., Bland-Hawthorn, J., Bridges, T., Cannon, R., Colless, M., Collins, C., Couch, W., Dalton, G., De Propriis, R., Driver, S. P., Efstathiou, G., Ellis, R. S., Glazebrook, K., Jackson, C., Lahav, O., Lewis, I., Lumsden, S., Madgwick, D., Peterson, B. A., Sutherland, W., & Taylor, K. 2001, *MNRAS*, 328, 64
- Norberg, P., Cole, S., Baugh, C. M., Frenk, C. S., Baldry, I., Bland-Hawthorn, J., Bridges, T., Cannon, R., Colless, M., Collins, C., Couch, W., Cross, N. J. G., Dalton, G., De Propriis, R., Driver, S. P., Efstathiou, G., Ellis, R. S., Glazebrook, K., Jackson, C., Lahav, O., Lewis, I., Lumsden, S., Maddox, S., Madgwick, D., Peacock, J. A., Peterson, B. A., Sutherland, W., & Taylor, K. 2002b, *MNRAS*, 336, 907
- Park, C., Choi, Y.-Y., Vogeley, M. S., Gott, J. R. I., & Blanton, M. R. 2007, *ApJ*, 658, 898
- Patrii, S. G., Betancort-Rijo, J. E., Prada, F., Klypin, A., & Gottlöber, S. 2006, *MNRAS*, 369, 335
- Peacock, J. A. & Smith, R. E. 2000, *MNRAS*, 318, 1144
- Peebles, P. J. E. 2001, *ApJ*, 557, 495
- Porciani, C. & Norberg, P. 2006, *MNRAS*, submitted
- Postman, M. & Geller, M. J. 1984, *ApJ*, 281, 95
- Rojas, R. R., Vogeley, M. S., Hoyle, F., & Brinkmann, J. 2004, *ApJ*, 617, 50
- . 2005, *ApJ*, 624, 571
- Scoccimarro, R., Sheth, R. K., Hui, L., & Jain, B. 2001, *ApJ*, 546, 20
- Seljak, U. 2000, *MNRAS*, 318, 203
- Seljak, U. & Zaldarriaga, M. 1996, *ApJ*, 469, 437
- Sheth, R. K., Mo, H. J., & Tormen, G. 2001, *MNRAS*, 323, 1
- Sheth, R. K. & Tormen, G. 2004, *MNRAS*, 350, 1385
- Skibba, R., Sheth, R. K., Connolly, A. J., & Scranton, R. 2006, *MNRAS*, 369, 68
- Spergel, D. N., Bean, R., Dore, O., Nolta, M. R., Bennett, C. L., Hinshaw, G., Jarosik, N., Komatsu, E., Page, L., Peiris, H. V., Verde, L., Barnes, C., Halpern, M., Hill, R. S., Kogut, A., Limon, M., Meyer, S. S., Odegard, N., Tucker, G. S., Weiland, J. L., Wollack, E., & Wright, E. L. 2006, *ApJ*, submitted, (astro-ph/0603449)
- Springel, V., White, S. D. M., Jenkins, A., Frenk, C. S., Yoshida, N., Gao, L., Navarro, J., Thacker, R., Croton, D., Helly, J., Peacock, J. A., Cole, S., Thomas, P., Couchman, H., Evrard, A., Colberg, J., & Pearce, F. 2005, *Nature*, 435, 629
- Tinker, J. L., Norberg, P., Weinberg, D. H., & Warren, M. S. 2007, *ApJ*, 659, 877
- Tinker, J. L., Weinberg, D. H., & Warren, M. S. 2006, *ApJ*, 647, 737
- Tinker, J. L., Weinberg, D. H., Zheng, Z., & Zehavi, I. 2005, *ApJ*, 631, 41
- Vogele, M. S., Geller, M. J., Park, C., & Huchra, J. P. 1994, *AJ*, 108, 745
- Warren, M. S. & Salmon, J. K. 1993, in *Supercomputing '93*
- Wechsler, R. H., Zentner, A. R., Bullock, J. S., Kravtsov, A. V., & Allgood, B. 2006, *ApJ*, 652, 71
- Weinmann, S. M., van den Bosch, F. C., Yang, X., Mo, H. J., Croton, D. J., & Moore, B. 2006, *MNRAS*, 372, 1161
- Wetzel, A. R., Cohn, J. D., White, M., Holz, D. E., & Warren, M. S. 2007, *ApJ*, 656, 139
- Yang, X., Mo, H. J., Jing, Y. P., & van den Bosch, F. C. 2005, *MNRAS*, 358, 217
- Yang, X., Mo, H. J., & van den Bosch, F. C. 2006, *ApJ*, 638, L55
- York, D. G. et al. 2000, *AJ*, 120, 1579
- Zehavi, I., Weinberg, D. H., Zheng, Z., Berlind, A. A., Frieman, J. A., Scoccimarro, R., Sheth, R. K., Blanton, M. R., Tegmark, M., Mo, H. J., et al. 2004, *ApJ*, 608, 16
- Zehavi, I., Zheng, Z., Weinberg, D. H., Frieman, J. A., Berlind, A. A., Blanton, M. R., Scoccimarro, R., Sheth, R. K., Strauss, M. A., Kayo, I., Suto, Y., Fukugita, M., Nakamura, O., Bahcall, N. A., Brinkmann, J., Gunn, J. E., Hennessy, G. S., Ivezić, Ž., Knapp, G. R., Loveday, J., Meiksin, A., Schlegel, D. J., Schneider, D. P., Szapudi, I., Tegmark, M., Vogeley, M. S., & York, D. G. 2005, *ApJ*, 630, 1
- Zheng, Z. 2004, *ApJ*, 610, 61
- Zhu, G., Zheng, Z., Lin, W. P., Jing, Y. P., Kang, X., & Gao, L. 2006, *ApJ*, submitted, (astro-ph/0601120)